〔生化学　第84巻　第8号，pp. 699–706，2012〕

特集：肝臓の発生・再生

ヒト肝細胞キメラマウス—肝臓肥大のメカニズムに関して—

立　野　知　世

我々は，ヒト肝細胞を持つキメラマウスを開発した．キメラマウス肝臓は，ヒト肝細胞とマウス非実質細胞で構築されている．キメラマウス肝臓のヒト肝細胞はヒト肝臓におけるヒト肝細胞に近い遺伝子発現，タンパク質発現，活性を示し，組織学的にもほぼ正常な肝臓組織構築を呈している．しかしながら，ヒト肝細胞キメラマウスでは，正常なヒトやマウスとは異なる性質も示す．その一つとして，肝臓の肥大が挙げられる．本稿では，ヒト肝細胞キメラマウスとラット肝細胞キメラマウスでの肝細胞の増殖，遺伝子，タンパク質発現を比較することにより，肝臓肥大のメカニズムに関して考察する．

1. はじめに

肝臓は，成体の肝臓を2/3切除しても残余肝が増殖し，げっ歯類では1週間で元の重量に戻ることから，成体になってもなお高い増殖能力を持つ臓器として知られている．しかしながら，肝細胞をコラゲナーゼ灌流法で分離し *in vitro* で培養すると，その高い増殖能を再現させることは現在のところ不可能である．また，肝細胞を2次元培養することにより，多くの遺伝子やタンパク質の発現が低下する．このことから，特にヒト肝細胞の *in vivo* での増殖・分化に関する性質は不明な点が多い．

Heckelらは生まれながら肝細胞の増殖に障害のあるトランスジェニックマウスを作製した．アルブミンエンハンサー／プロモーター下にウロキナーゼ型プラスミノーゲンアクチベーター（urokinase-type plasminogen activator, uPA）のゲノム遺伝子が約5個連結された形でベクターが導入されているトランスジェニックマウス（Alb-uPAマウス）である[1]．Rhimらは生後5～11日目のAlb-uPAマウスの脾臓から正常なマウス肝細胞を移植すると，移植したマウス肝細胞が宿主であるAlb-uPAマウスの肝臓に生着・増殖し完全に置換することを示した[2]．彼らはさらにAlb-uPAマウスとヌードマウスを掛け合わせることにより，Alb-uPA/ヌードマウスを作製し，ラット肝細胞で置換された肝臓を持つキメラマウスを作製した[3]．その後，筆者らも含めいくつかのグループにより，Alb-uPA/SCIDマウス[4,5]やAlb-uPA/Rag2ノックアウト[6]マウスなどが作製され，ヒト肝細胞によるマウス肝臓の置換の試みが行われた．

筆者らは他のグループに先立ち，マウス肝臓のほとんどがヒト肝細胞で置換されたキメラマウス（ヒト肝細胞キメラマウス）を安定的に生産することに成功した[4]．このマウスは，ヒト型の薬物代謝能を持つことや[4,7,8]，B型肝炎ウイルス（HBV）やC型肝炎ウイルス（HCV）に感染可能であることから[5,6]，新薬開発のための薬物代謝試験や抗HBV薬や抗HCV薬の薬効試験に使われている．

筆者らは，このヒト肝細胞キメラマウスは，*in vivo* におけるヒト肝細胞の増殖・分化能に関する研究に有用と考えている．また，ヒト肝細胞キメラマウスの肝臓では，肝細胞はヒト由来であるが，非実質細胞はマウス由来である．ヒト肝細胞キメラマウスにおけるヒト肝細胞が通常とは異なる環境におかれることにより生じる異常現象を解明することにより，肝細胞と非実質細胞，肝細胞と他組織との新たな相互作用を知りえるのではないかと考えている．本稿では，ヒト肝細胞キメラマウスで観察される異常な性質の一つである，肝重量体重比の増加について取り上げ，肝重量体重比調節メカニズムに関して考察する．

株式会社フェニックスバイオ（〒739-0046 広島県東広島市鏡山3-4-1）

Chimeric mice with humanized liver—Mechanism of hepatic hyperplasia induction—

Chise Tateno (PhoenixBio Co., Ltd., 3-4-1 Kagamiyama, Higashihiroshima, Hiroshima 739-0046, Japan)

2. ヒト肝細胞キメラマウスの作製とその利用

筆者らはAlb-uPAマウス[1]と重度免疫不全のSCIDマウスを掛け合わせたAlb-uPA/SCIDマウスを作製し[4]，現在クローズドコロニーとして株式会社フェニックスバイオにおいて系統を維持している．約3週齢のAlb-uPA/SCIDマウスに脾臓経由で米国から購入した子供のドナー由来の凍結保存ヒト肝細胞を融解後2.5～10×10^{5}個注入すると，約2ヶ月でマウス肝臓の70%以上がヒト肝細胞で置換されたキメラマウスが作出できる（図1）．ヒト肝細胞を移植後，経時的にマウス血液を採取しマウス血中ヒトアルブミン濃度のモニタリングを行っている．移植後7週目（10週齢）頃まで対数的にヒトアルブミン濃度は増加するがその後安定する（図1）．マウス肝臓の7葉の組織切片を作製し，ヒト特異的サイトケラチン8/18抗体を用いて免疫染色を行い，マウス肝臓のヒト肝細胞による置換率を求めている（図2）．屠殺時のマウス血中ヒトアルブミン濃度と置換率はよく相関していることから，ヒトアルブミン濃度からマウスの置換率を推定することができる（図1）．

ヒト肝細胞キメラマウス肝臓はヒト肝臓と同等の薬物代謝酵素やトランスポーターを発現していることから[4,7,8]，新薬におけるヒト薬物代謝予測に利用されている．これまで *in vivo* でのHBVやHCVの新薬の薬効試験にはチンパンジーが使われていたが，最近では動物愛護の問題からその使用が難しくなってきている．ヒト肝細胞キメラマウスはHBVやHCVに容易に感染することができるため[5,6]，現在唯一のHBV，HCV感染小動物モデル系として利用されている．

現在，株式会社フェニックスバイオでは，移植したマウスの約8割が置換率70%以上の高置換のキメラマウスを大量生産することが可能である．年間約3,000匹のヒト肝細胞キメラマウスを生産し，これらのマウスは学術研究機関や製薬会社との共同研究や受託試験に使われている．

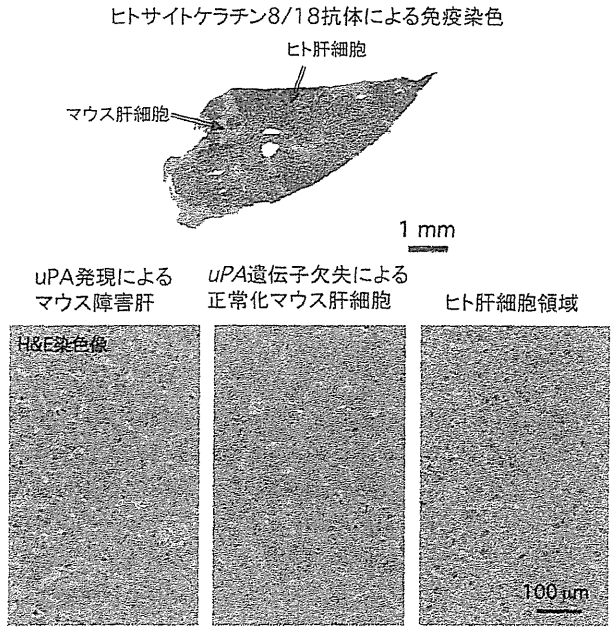

図2 ヒト肝細胞キメラマウスの組織像

3. ヒト肝細胞キメラマウスの特徴

ヒト肝細胞キメラマウス肝臓は，ヒト肝細胞とマウス由来の類洞内皮細胞，クッパー細胞，星細胞などの非実質細胞で構成されている．キメラマウス肝臓切片をヘマトキシリン・エオシン（H&E）染色すると，3種類の肝細胞が観察できる（図2）．1）uPAの発現による障害マウス肝細胞

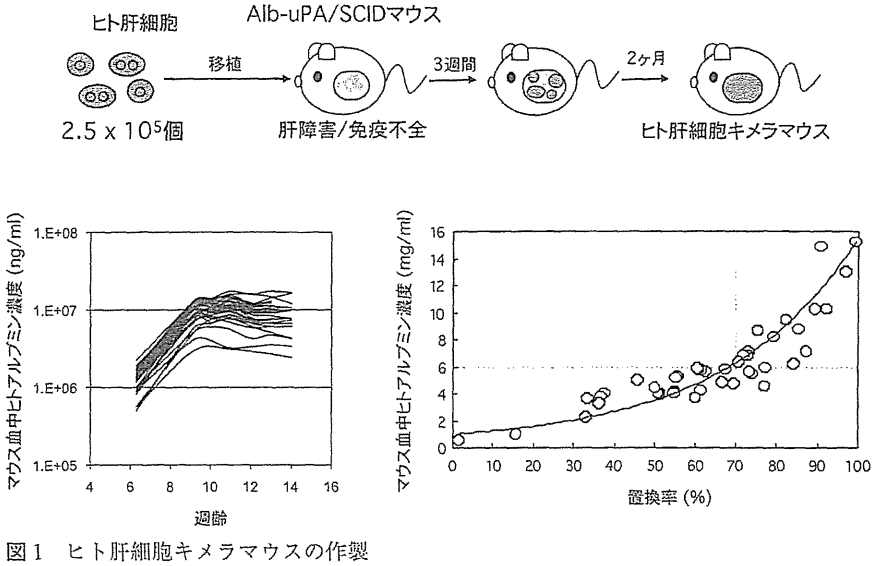

図1 ヒト肝細胞キメラマウスの作製

であり，萎縮している．細胞質に多くの小さな脂肪滴を持つ．2）肝細胞の細胞分裂の際に，導入された *uPA* 遺伝子が相同組換えにより欠失することにより正常化したマウス肝細胞である．細胞質がエオシンに好染し正常マウス肝細胞の形態を示す．3）マウス肝臓を置換したヒト肝細胞である．マウス正常肝細胞に比べて核の大きさが均一で小型であり，細胞質が淡明である．細胞質が過ヨウ素酸シッフ（PAS）染色陽性であることから，ヒト肝細胞にグリコーゲンが多く存在しているためと考えられる．これら3種の細胞の特徴は透過型電子顕微鏡でも確認できる．電子顕微鏡観察により，ヒト肝細胞領域においても，正常な類洞構造が形成されており，肝細胞と類洞内皮細胞間にはディッセ腔が存在することが確認できる．また，肝細胞間には胆汁が分泌される毛細胆管が形成されている．後に詳細に述べるが，正常なげっ歯類やヒト肝臓では，肝細胞が類洞に沿って1列に並んでいるが，ヒト肝細胞キメラマウスでは，2列に並んでいる[9]．

これらのことから，ヒト肝細胞とマウス非実質細胞はほぼ正常に構築されていると考えている．また，遺伝子発現の観点から観察すると，ヒト肝臓由来の肝細胞とヒト肝細胞由来の肝細胞の遺伝子発現をマイクロアレイで比較することにより，80～85%の遺伝子が2倍の範囲内で同等の発現をしていることを確認している．

ヒト肝細胞キメラマウスの持つ正常なヒトやマウスと異なる性質もいくつか明らかになっている．ヒト肝細胞キメラマウスは肝重量体重比が正常のマウスに比べて1.5～2.0倍高い[9]（図3）．通常，体重に対する臓器重量は動物種により決まっており，部分肝切除後も元の重量に戻る[10~12]．肝重量体重比は，マウスでは約5～6%[9]，ラットでは約3.5～4.5%[11]，ヒトでは約2～3%[12]ということが知られている．また，ヒト肝細胞キメラマウスでは血清中の胆汁酸濃度が正常マウスに比べて高いという特徴も持つ．

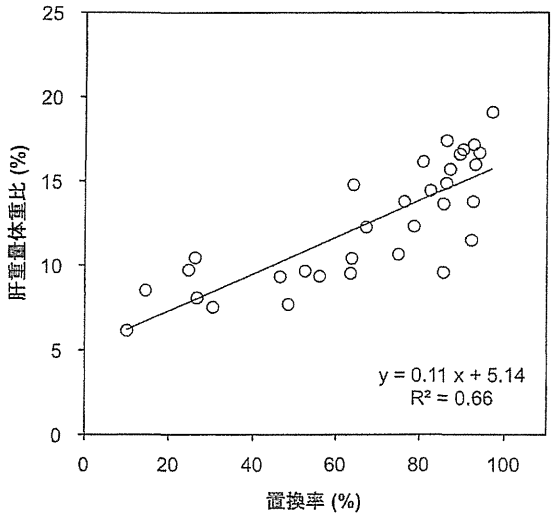

図3 ヒト肝細胞キメラマウス肝臓の肥大化

4. マウス肝細胞およびラット肝細胞キメラマウスを用いたG1からS期への移行メカニズムの探索

Weglarzらは，主要尿タンパク（major urinary protein, MUP）のプロモーターを用いたuPAトランスジェニックマウスを作製した[13]．MUPプロモーターは生後発現するという以外は，これまでのuPAマウスと同様な特徴を持つ．このMUP-uPAマウスとヌードマウスを掛け合わせ，MUP-uPA/ヌードマウスを作製した[14]．

2/3部分肝切除後のDNA合成が亢進した肝細胞の動態は，ラットとマウスで異なることが知られている．ラットでは，術後24時間と36時間に二つのピークがある．一方，マウスでは，40時間後に一つのピークがあることが知られている[14]．ラット肝細胞はマウスの体内に存在すると，どちらの動態を示すのだろうか．この疑問に答えるために，彼らは，MUP-uPA/ヌードマウスにラット肝細胞とマウス肝細胞を移植し，キメラマウスを作製した[14]．作製したラット肝細胞キメラマウスとマウス肝細胞キメラマウスに2/3肝部分切除術を施し，その後の肝細胞におけるDNA合成能をブロモデオキシウリジン（BrdU）の取り込みにより調べた．その結果，ラット肝細胞キメラマウスは，24時間と36時間，二つのピークを示し，コントロールのマウス肝細胞キメラマウスでは，マウスと同様40時間にピークを示した[14]．このことから，G1からS期への移行は，サイトカインや増殖因子による外因的な刺激よりも，内因的な性質によることが証明された．

5. ヒトおよびラット肝細胞キメラマウスの作製

筆者らは，ヒト肝細胞キメラマウスにおける肝臓の肥大メカニズムを調べるために，Alb-uPA/SCIDマウスに7.5×10^5個のヒト肝細胞と5.0×10^5個のラット肝細胞を移植し，ヒト肝細胞キメラマウスとラット肝細胞キメラマウスを作製した．移植後1週目よりマウスを安楽死させ，肝臓のサンプリングを行い肝重量体重比および置換率を求めた．さらに肝臓におけるBrdUの取り込みとタンパク質発現を免疫染色により，また，遺伝子発現を定量性リアルタイムRT-PCR法により測定した．

6. ヒトおよびラット肝細胞キメラマウスの肝重量体重比

肝重量体重比を調べると，ラット肝細胞キメラマウスは5.4%とほぼ正常マウスと同じであったが，ヒト肝細胞キメラマウスは，マウス肝臓におけるヒト肝細胞の置換率が上昇するとともに肝重量体重比が増加し，置換率約80%以上では約13%の肝重量体重比であった（図3）．また，肝臓の肥大が個々の肝細胞の肥大によるものか，肝細胞数の増加によるものかを調べるために，一定面積あたりの肝

細胞数を計測した．その結果，肝細胞自身の肥大は観察されなかったことから，ヒト肝細胞キメラマウス肝臓の肥大は肝細胞数の増加であると結論した[9]．

7. ヒトおよびラット肝細胞キメラマウス肝細胞増殖の動態

ラット肝細胞キメラマウスとヒト肝細胞キメラマウスの血中ラットおよびヒトアルブミン濃度と肝臓におけるBrdUの取り込みを調べた．ラット肝細胞キメラマウスは移植後1週目で約15%であったがその後急速に低下し4週で正常マウスレベルに達し，置換率は100%となった．一方，ヒト肝細胞キメラマウスではBrdUの取り込みは移植後1週目で約10%であったが，その後ゆるやかに減少し11週で正常マウスレベルに達し，置換率は平均で約60%であった[9]（図4）．

これらのことから，ラットに比べてヒトでは肝細胞の増殖速度が遅いと考えられた．系統発生学的にラットとマウスは近縁であり，ヒトとマウスは遠縁であるため，サイトカインなどのアミノ酸配列に関しては，前者に比べて後者は相同性が低いと考えられる．このことから，ラットとヒト肝細胞の増殖能として同列に比較することはできないが，これまでの肝部分切除後の再生速度の報告からは，ラットでは約7日で元の重量まで再生するのに対し，ヒトでは約1ヶ月かかると言われていることから，ヒトにおける増殖速度の遅さをある程度反映しているものと考えている．

8. 肝部分切除における増殖の停止機構

肝臓再生における増殖の停止のメカニズムにはトランスフォーミング増殖因子β（TGF-β）やアクチビンが関わっていることが知られている[15,16]．TGF-βはまずTGF-β受容体2（TGFBR2）の二量体に結合しTGFBR2をリン酸化する．さらにTGF-β受容体1（TGFBR1）が結合することにより，TGFBR1がリン酸化される．Smad2/3がその後リン酸化され，Smad4と複合体を形成し核内移行する．核内で転写因子とともにDNAドメインに結合することにより，DNA合成が低下し，アポトーシスが誘導され，肝細胞の増殖は停止すると言われている．肝部分切除では，切除後すみやかに肝細胞のTGFBRの発現が低下し，非実質細胞のTGF-βの発現は増加する．切除後120時間後には肝細胞のTGFBRの発現は上昇し元に戻ることが知られている[17]．

9. ヒトおよびラット肝細胞キメラマウス肝細胞のTGFBRファミリーの発現

ヒト肝細胞キメラマウスでは正常な増殖停止機構が働いているのかどうかを調べるために，TGFBRファミリーのラットおよびヒト肝細胞キメラマウス肝臓におけるmRNA発現量を経時的に計測した．ラット肝細胞キメラマウスでは，移植後2週目において，ラット（r)TGFBR1，rTGFBR2，ラットアクチビン受容体2A（rACTR2A）の発

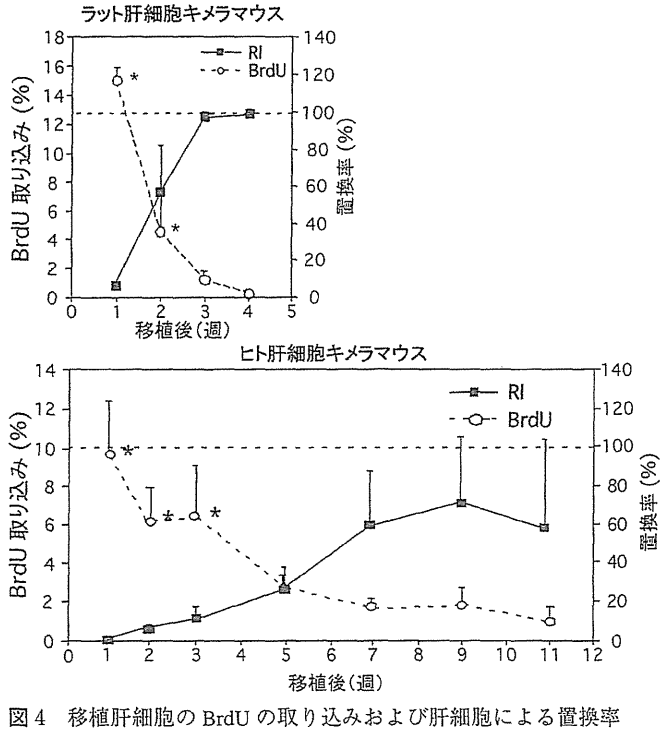

図4 移植肝細胞のBrdUの取り込みおよび肝細胞による置換率（文献9を改変）

現は約半分に低下しており，増殖の停止時点である3週目より正常値に戻っていた（図5）．一方，ヒト肝細胞キメラマウスでは，移植後3週目において，ヒト（h）TGFBR1，hTGFBR2，hACTR2Aの発現は0.1〜0.4倍に低下していた．hTGFBR1は移植後11週目において正常値に戻ったが，hTGFBR2，hACTR2Aは低値のままであった[9]（図5）．

次にTGFBR2，Smad2，Smad3のタンパク質発現を免疫染色により調べた．その結果，増殖停止時期である移植後3週目のラット肝細胞キメラマウス肝臓では，TGFBR2の細胞質における発現が見られ（図6），同時期にSmad2，Smad3の核内移行が観察された（図7）．一方，ヒト肝細胞キメラマウスでは，増殖の停止期である移植後11週目

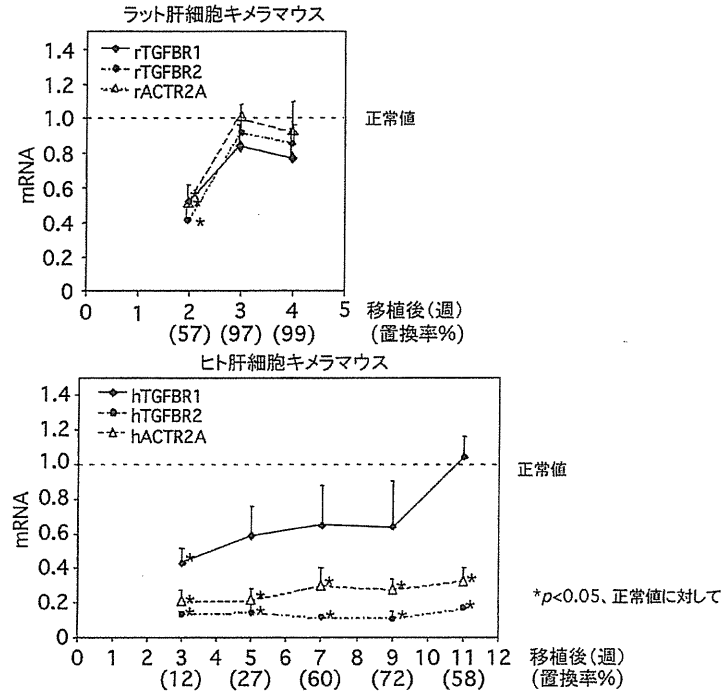

図5 肝細胞移植後のTGFBR，ACTRのmRNA量の変化（文献9を改変）

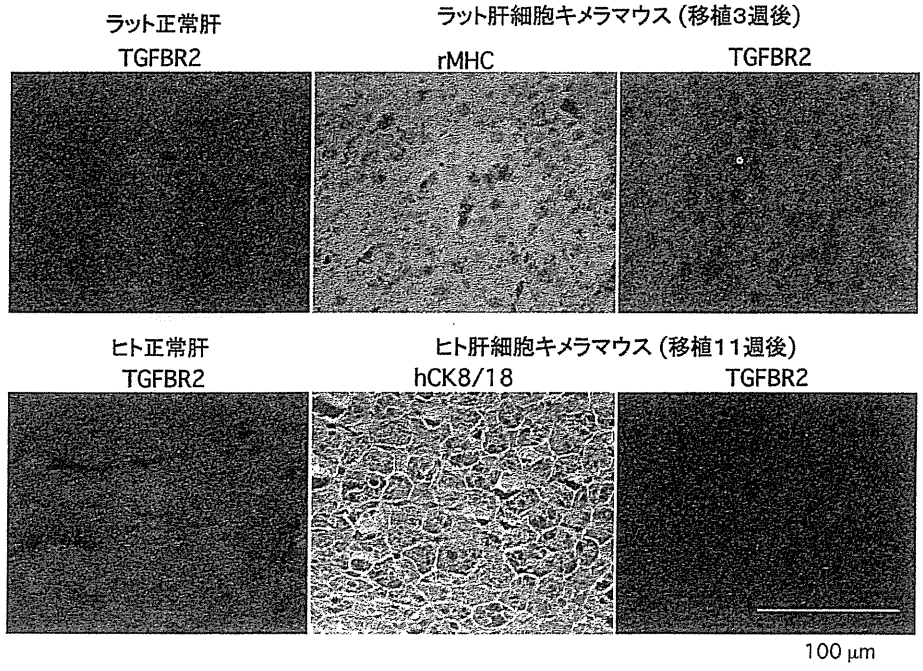

図6 TGFBR2の免疫染色（文献9を改変）

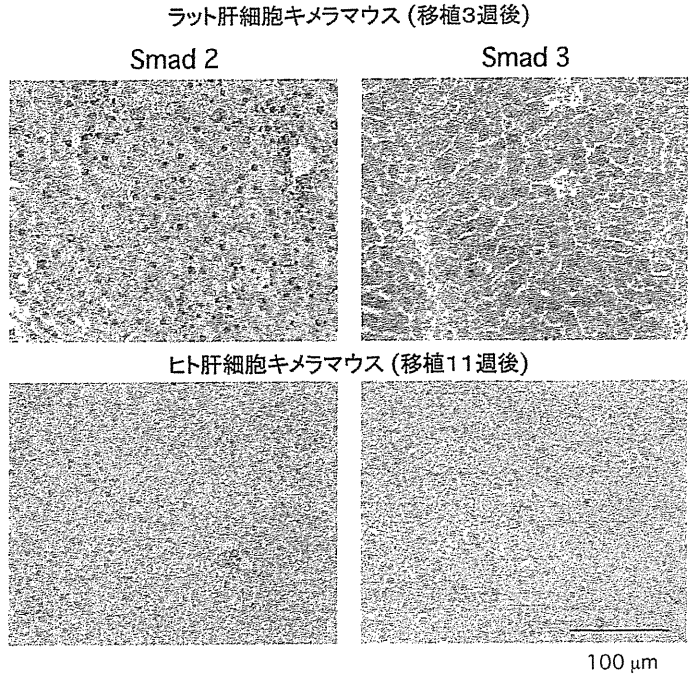

図7 Smad2，3の免疫染色（文献9を改変）

において，TGFBR2の細胞質における発現は低く（図6），Smad2，Smad3の核内移行も観察されなかった（図7）．また，E-カドヘリンとβ1-インテグリンはSmad2/3を介したTGF-βシグナルのターゲット遺伝子であることが知られている[18]．ヒト肝細胞キメラマウス肝臓においては，E-カドヘリンのタンパク質発現が正常ヒト肝臓に比べて低いことが示され，TGF-βシグナルが働いていないと考えられた[9]．

10. ヒトおよびラット肝細胞キメラマウスの肝細胞索構造

IV型コラーゲンの抗体で正常マウス，ラット，ヒト肝臓を染色すると，肝細胞は1列の索状構造を形成しているのが観察される（図8）．移植2週目のヒトおよびラット肝細胞キメラマウス肝臓を，同様に染色すると，どちらも肝細胞索を形成しておらず，コロニー状に存在していた．ラット肝細胞キメラマウス肝臓では，増殖の停止した移植後5週目では，IV型コラーゲン染色により，正常肝と同様な1列の肝細胞索が観察された．ところが，ヒト肝細胞キメラマウスでは，増殖の停止した移植後14週でも肝細胞索は2〜3列となっていた[9]（図8）．再生肝では肝細胞索が2列であることが知られていることから[19]，ヒト肝細胞キメラマウスでは，DNA合成は停止しているものの，再生肝の特徴を維持していると考えられた．

11. 宿主マウス星細胞におけるTGF-βの発現

部分肝切除後約120時間後には，星細胞がTGF-βを産生し，再生の停止に寄与していると考えられている[16]．また，正常肝では，TGF-βの発現はほとんど見られない．ラット肝細胞キメラマウスの星細胞におけるTGF-βの発現を免疫染色により調べた．その結果，移植後2週目ではデスミン陽性星細胞でのTGF-βの発現はみられなかったが，3週目においては，デスミン陽性星細胞でのTGF-βの発現が観察された．一方，ヒト肝細胞キメラマウスの肝臓では，移植後5週でも11週目においても，デスミン陽性

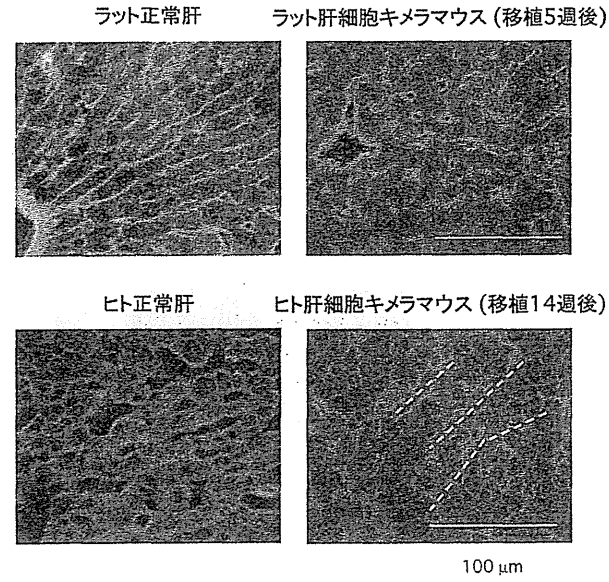

図8 IV型コラーゲンの免疫染色（文献9を改変）

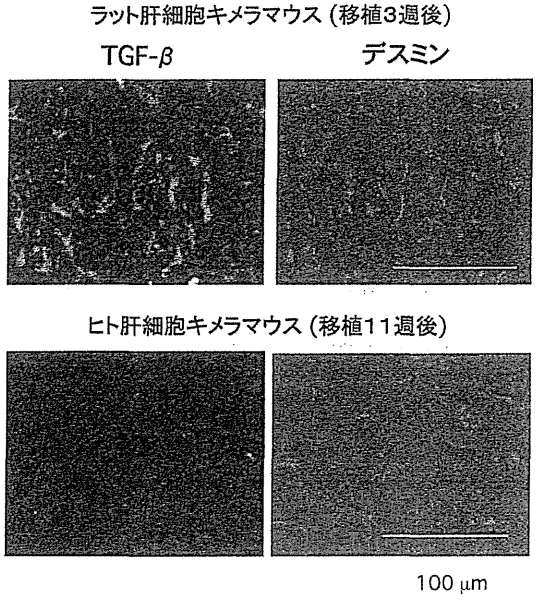

図9 TGF-β/デスミンの免疫染色（文献9を改変）

星細胞でのTGF-βの発現は見られなかった[9]（図9）．このことから，ヒト肝細胞キメラマウス肝臓では，ヒト肝細胞におけるTGFBR2，ACTR2の発現のみでなく，星細胞におけるTGF-βも発現していないことが明らかとなった．

12. 胆汁酸による肝重量体重比への影響

肝重量体重比の調節因子の一つとして，胆汁酸が挙げられる．マウスに胆汁酸（0.2%）を餌に混ぜて与えると，肝細胞へのBrdUの取り込みが増加し，肝重量体重比が30%上昇する．この反応には肝細胞の核内受容体であるファルネソイドX受容体（FXR）が関与している．胆汁酸はFXRを介してFoxM1B転写因子を誘導し，肝細胞の増殖を促進する．一方，FXRは核内受容体であるショートヘテロダイマーパートナー（SHP）を誘導し，胆汁酸合成酵素であるCyp7a1の発現を抑え，胆汁酸合成を低下させる．肝部分切除後，血中の胆汁酸がやや増加し，それに伴い，SHPの増加，Cyp7a1の低下が見られ，部分肝切除7日目には正常に戻る[20]．これらのことから，胆汁酸は肝重量体重比の調節に関わっているのではないかと考えられる．ヒト肝細胞キメラマウス血清中では，胆汁酸濃度が正常マウスに比べて高く，また，CYP7A1の発現も高い．このことから，ヒト肝細胞キメラマウスでは何らかの原因で胆汁酸産生調節に不具合が生じており，マウス血中胆汁酸が低下しないことが肝重量体重比の増加に関わっているのかもしれない．

13. おわりに

肝細胞の増殖に関わる増殖因子，サイトカイン，ホルモンに対する受容体が肝細胞表面に存在する場合，ヒト肝細胞キメラマウスでは，アミノ酸配列のホモロジーの種差により通常起きている反応が起こらないという可能性がある．その一つの例として，成長ホルモンが挙げられる．

ヒト成長ホルモン（hGH）は，マウスの成長ホルモン受容体（mGHR）に結合しないことが知られている[21]．肝臓の再生には，GHによる肝細胞の増殖促進作用が関わっていることが，GHノックアウトマウスなどを用いた実験により明らかになっている．ヒト肝細胞キメラマウスでは，マウスの下垂体から放出されるmGHは存在するが，hGHは存在しない[22]．hGHが存在しないことにより，ヒト肝細胞キメラマウスではヒト肝細胞に脂肪肝が生じる．キメラマウスにhGHを投与することにより脂肪肝やhGH欠損による遺伝子発現の異常が正常化する[23]．

ヒト肝細胞キメラマウスにおける肝臓肥大に関しても，このような種差による何らかの原因があり，それを是正することにより，より正常に近いヒト肝臓を持つキメラマウスを作製できるのではないかと考えている．

謝辞

本研究に主に携わられた現東京女子医科大学の鵜頭理恵先生，御指導くださいました現株式会社フェニックスバイオ吉里勝利先生に深く感謝致します．また，本研究は知的クラスター創成事業と株式会社フェニックスバイオにおいて実施された．

文 献

1) Heckel, J.L., Sandgren, E.P., Degen, J.L., Palmiter, R.D., & Brinster, R.L. (1990) *Cell*, 62, 447–456.
2) Rhim, J.A., Sandgren, E.P., Degen, J.L., Palmiter, R.D., & Brinster, R.L. (1994) *Science*, 263, 1149–1152.
3) Rhim, J.A., Sandgren, E.P., Palmiter, R.D., & Brinster, R.L. (1995) *Proc. Natl. Acad. Sci. USA*, 92, 4942–4946.
4) Tateno, C., Yoshizane, Y., Saito, N., Kataoka, M., Utoh, R., Yamasaki, C., Tachibana, A., Soeno, Y., Asahina, K., Hino, H., Asahara, T., Yokoi, T., Furukawa, T., & Yoshizato, K. (2004) *Am. J. Pathol.*, 165, 901–912.
5) Mercer, D.F., Schiller, D.E., Elliott, J.F., Douglas, D.N., Hao, C., Rinfret, A., Addison, W.R., Fischer, K.P., Churchill, T.A., Lakey, J.R.T., Tyrrell, D.L.J., & Kneteman, N.M. (2001) *Nat. Med.*, 7, 927–933.
6) Dandri, M., Burda, M.R., Török, E., Pollok, J.M., Iwanska, A., Sommer, G., Rogiers, X., Rogler, C.E., Gupta, S., Will, H., Greten, H., & Petersen, J. (2001) *Hepatology*, 33, 981–988.
7) Katoh, M., Matsui, T., Okamura, H., Nakajima, M., Nishimura, M., Naito, S., Tateno, C., Yoshizato, K., & Yokoi, Y. (2005) *Drug Metab. Dispos.*, 33, 1333–1340.
8) Nishimura, M., Yoshitsugu, H., Yokoi, T., Tateno, C., Kataoka, M., Horie, T., Yoshizato, K., & Naito, S. (2005) *Xenobiotica*, 35, 877–890.
9) Utoh, R., Tateno, C., Kataoka, M., Tachibana, A., Masumoto, N., Yamasaki, C., Shimada, T., Itamoto, T., Asahara, T., &

Yoshizato, K. (2010) *Am. J. Pathol.*, 177, 654–665.
10) Kam, I., Lynch, S., Svanas, G., Todo, S., Polimeno, L., Francavilla, A., Penkrot, R.J., Takaya, S., Ericzon, B.G., Starzl, T. E., & Van Thiel, D.H. (1987) *Hepatology*, 7, 362–366.
11) Francavilla, A., Zeng, Q., Polimeno, L., Carr, B.I., Sun, D., Porter, K.A., Van Thiel, D.H., & Starzl, T.E. (1994) *Hepatology*, 19, 210–216.
12) Van Thiel, D.H., Gavaler, J.S., Kam, I., Francavilla, A., Polimeno, L., Schade, R.R., Smith, J., Diven, W., Penkrot, R.J., & Starzl, T.E. (1987) *Gastroenterology*, 93, 1414–1419.
13) Weglarz, T.C., Degen, J.L., & Sandgren, E.P. (2000) *Am. J. Pathol.*, 157, 1963–1974.
14) Weglarz, T.C. & Sandgren, E.P. (2000) *Proc. Natl. Acad. Sci. USA*, 97, 12595–12600.
15) Hu, P.P., Datto, M.B., & Wang, X.F. (1998) *Endocr. Rev.*, 19, 349–363.
16) Braun, L., Mead, J.E., Panzica, M., Mikumo, R., Bell, G.I., & Fausto, N. (1988) *Proc. Natl. Acad. Sci. USA*, 85, 1539–1543.
17) Chari, R.S., Price, D.T., Sue, S.R., Meyers, W.C., & Jirtle, R. L. (1995) *Am. J. Surg.*, 169, 126–132.
18) Weinstein, M., Monga, S.P., Liu, Y, Brodie, S.G., Tang, Y., Li, C., Mishra, L., & Deng, C.X. (2001) *Mol. Cell Biol.*, 21, 5122–5131.
19) Wack, K.E., Ross, M.A., Zegarra, V., Sysko, L.R., Watkins, S. C., & Stolz, D.B. (2001) *Hepatology*, 33, 363–378.
20) Huang, W., Ma, K., Zhang, J., Qatanani, M., Cuvillier, J., Liu, J., Dong, B., Huang, X., & Moore, D.D. (2006) *Science*, 312, 233–236.
21) Souza, S.C., Frick, G.P., Wang, X., Kopchick, J.J., Lobo, R.B., & Goodman, H.M. (1995) *Proc. Natl. Acad. Sci., USA*, 92, 959–963.
22) Masumoto, N., Tateno, C., Tachibana, A., Utoh, R., Morikawa, Y., Shimada, T., Momisako, H., Itamoto, T., Asahara, T., & Yoshizato, K. (2007) *J. Endocrinol.*, 194, 529–539.
23) Tateno, C., Kataoka, M., Utoh, R., Tachibana, A., Itamoto, T., Asahara, T., Miya, F., Tsunoda, T., & Yoshizato, K. (2011) *Endocrinology*, 152, 1479–1491.

SCIENTIFIC REPORTS

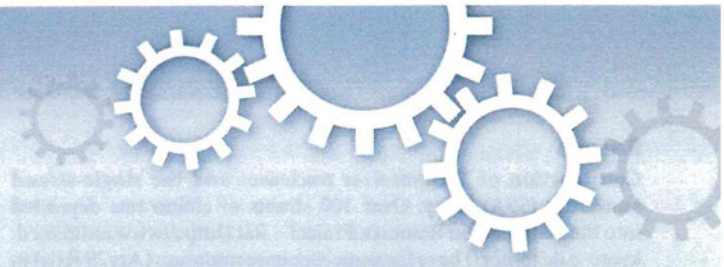

OPEN

SUBJECT AREAS:
GENE TARGETING
TRANSGENIC ORGANISMS
GENETIC ENGINEERING
MUTAGENESIS

Received
31 October 2012

Accepted
4 January 2013

Published
13 February 2013

Correspondence and requests for materials should be addressed to T.M. (tmashimo@anim.med.kyoto-u.ac.jp)

Efficient gene targeting by TAL effector nucleases coinjected with exonucleases in zygotes

Tomoji Mashimo[1], Takehito Kaneko[1], Tetsushi Sakuma[2], Junya Kobayashi[3], Yayoi Kunihiro[1], Birger Voigt[1], Takashi Yamamoto[2] & Tadao Serikawa[1]

[1]Institute of Laboratory Animals, Graduate School of Medicine, Kyoto University, Kyoto 606-8501, Japan, [2]Department of Mathematical and Life Sciences, Graduate School of Science, Hiroshima University, Higashi-Hiroshima 739-8526, Japan, [3]Genome Repair Dynamics, Radiation Biology Center, Kyoto University, Kyoto 606-8501, Japan.

TAL Effector Nucleases (TALENs) are versatile tools for targeted gene editing in various species. However, their efficiency is still insufficient, especially in mammalian embryos. Here, we showed that combined expression of Exonuclease 1 (*Exo1*) with engineered site-specific TALENs provided highly efficient disruption of the endogenous gene in rat fibroblast cells. A similar increased efficiency of up to ~30% with *Exo1* was also observed in fertilized rat eggs, and in the production of knockout rats for the albino (*Tyr*) gene. These findings demonstrate TALENs with *Exo1* is an easy and efficient method of generating gene knockouts using zygotes, which increases the range of gene targeting technologies available to various species.

Genetically engineered animals provide a powerful tool for the functional annotation of genes and for modeling human genetic diseases. Advances over the past 20 years in mouse embryonic stem cells and homologous recombination (HR)-mediated targeting have made this species the first choice for modeling human diseases. However, these technologies were only available in mice, and not in other species. Recently, new technologies have been developed and tested for gene disruption, and HR could prove an invaluable tool for the rapid generation of genetically modified animals. These new approaches include zinc-finger nucleases (ZFNs), comprising the DNA-binding domain of zinc-finger proteins fused with the non-specific DNA endonuclease *Fok*I[1–4], and transcription activator-like effector nucleases (TALENs), comprising an engineered array of TAL effector repeats fused to the *Fok*I nuclease domain[5–8]. These engineered nucleases can recognize long stretches of DNA sequences and introduce DNA double-strand breaks (DSBs). DSBs are mainly restored via non-homologous end-joining (NHEJ), a process that introduces small insertions or deletions (indels) at the repair junction, thereby generating mutations at the targeted sequences[1–8]. They are especially useful in previously non-permissive model organisms, such as sea urchins[9], crickets[10], medaka fish[11], or rats[12–14].

ZFNs/TALENs provide a straightforward strategy for targeted gene disruption in zygotes, resulting in rapid and cost-effective knockouts. Although both commercial and open resources are available for the design of ZFN/TALEN reagents, ZFNs present hurdles in terms of cost and protocols, making it difficult to establish ZFNs as a routine laboratory process. The sequences recognized by ZF domains are also limited, whereas TAL effectors can recognize almost any sequence, except T at position 0[5,7,8]. Simple and straightforward design and assembly strategies have been developed for rapid construction of TALENs, providing a cost-effective targeted nuclease platform. Although TALEN technologies have advantages, the technology remains uncertain because its introduction is so recent[6]. Since the original discovery of TAL effectors in the plant pathogenic bacteria, *Xanthomonas*, the system appears to be less effective in rodent embryos, such as mice and rats (unpublished data, personal communication). The larger size of the proteins may also impede the gene targeting efficiency compared with ZFNs, even though the recently reported truncation of the N- and C-terminal regions of the native proteins has increased the TALEN DSB-activity[15]. Improved methodology is needed to further exploit the utility of this technology. For example, a recent report showed that coupling designer endonucleases with DNA end-processing enzymes could improve gene disruption rates in mouse and human cells[16]. To address this issue, we co-expressed Exonuclease 1 (*Exo1*) with engineered TALENs to enhance gene targeting efficiency in rat zygotes.

Results

Construction of TAL effecter nucleases and the single-strand annealing (SSA) assay. Over 100 strains of albino rats deposited into the National Bio Resource Project – Rat (http://www.anim.med.kyoto-u.ac.jp/nbr/) have the same missense mutation (Arg299His) in the Tyrosinase (*Tyr*) gene[17]. The coat-color phenotype is easily and observably distinguishable for TALEN-induced mutations; therefore, we targeted the rat *Tyr* gene. A pair of TALENs was constructed using a two-step assembly method[18] with a Golden Gate TALEN kit, originally established from the Voytas lab[19] (Figure 1A). For the subsequent use of TALENs in the SSA assay, transfection into cultured cells, and mRNA synthesis, the backbone vectors for the second-step assembly were replaced with the mammalian expression vector pcDNA-TAL vector, which has CMV and T7 promoters[18]. The TALEN-based constructs were also replaced with deletion frameworks of +153 N- and +47 C-terminal domains, termed the NC scaffold, as previously reported[15] (Figure 1B).

We then performed a validation test of the mammalian cell-based SSA assay in human embryonic kidney 293T (HEK293T) cells for designed Tyr-TALENs and Tyr-TALENs-NC (Figure 1C).

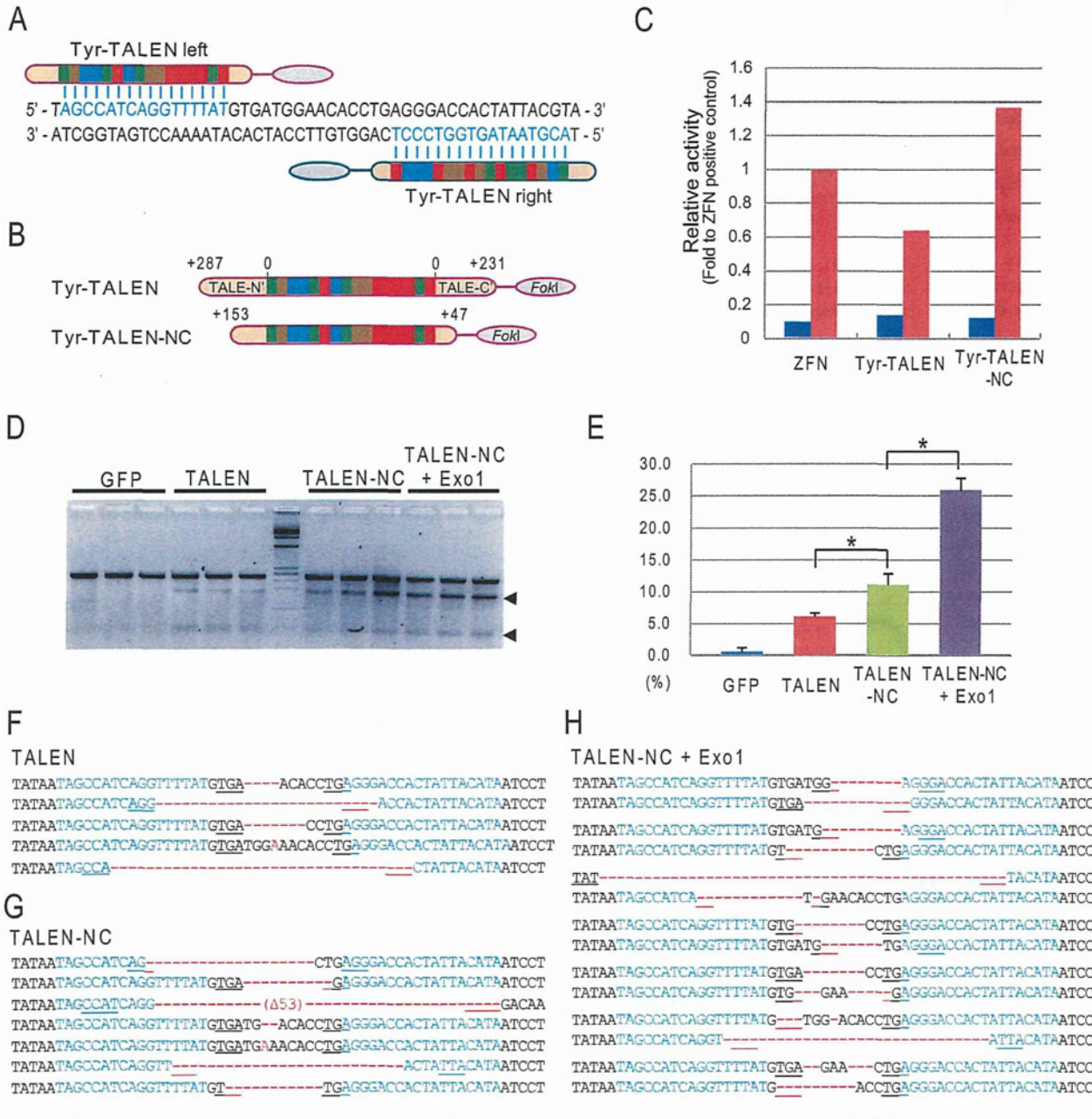

Figure 1 | TALEN constructs and the validation of their activity in rat fibroblasts. (A) Structure of engineered TALENs binding to exon 2 of rat Tyrosinase (*Tyr*) gene. (B) TALEN scaffolds (upper) and N- and C-terminal truncated scaffolds (lower), respectively. (C) Relative TALEN activity measured by a single-strand annealing (SSA) assay in human embryonic kidney 293T (HEK293T) cells. (D) Surveyor (Cel-I) nuclease assay for TALEN-induced mutations in *Tyr*. Arrowheads indicate the expected positions of the digested products. (E) Surveyor assay showing that increased frequency of TALEN-induced mutations by NC truncation and co-expression of *Exo1*. Data are expressed as means ± SEM (n = 3). *P<0.01 by Student's t-tests. (F–H) Sequence analyses showing increased mutation efficiency by NC truncation and *Exo1* expression. Microhomologous sequences adjacent to the breakpoint are underlined for TALEN (F), TALEN-NC (G), and TALEN-NC + *Exo1* (H).

Compared with the positive control (ZFN transfected cells[9]) and negative controls (reporter vectors with unrelated sequences), the cells transfected with Tyr-TALENs showed marked activation of the *luciferase* gene at about 60% of the value of the ZFN positive control. The cells transfected with Tyr-TALENs-NC showed 40% higher activity than the ZFN treated cells, indicating that the custom-engineered TALENs have the cleavage activity and that the NC truncation of TALENs increases the cleavage efficiency in the SSA assay (Figure 1C).

Combination of exonucleases with TALENs increased the efficiency of targeted gene disruption in rat fibroblasts. To assess the activity of the TALEN architectures against an endogenous gene, we electroporated Tyr-TALEN or Tyr-TALEN-NC expression vectors, and the GFP expression vector as a negative control, into Rat-1 fibroblast cells (Table 1). After 24 h, the control cells showed more than 90% GFP-positive cells, indicating sufficient transformation rates. After 72 h, cell numbers were counted, and genomic DNA was extracted and screened for TALEN-induced mutations using the Surveyor (Cel-I) nuclease assay (Figure 1D). Similar to the results of the SSA assay, TALENs-NC showed higher activity than TALENs (11.0% *vs.* 6.1%) in Rat-1 cells (Figure 1E). However, compared with our previous results using ZFNs (mutation rates ~25%[13,20]), the TALEN activity was significantly lower.

To increase the frequency of TALEN-induced mutations, we added vectors expressing the *Exo1* gene. Co-transfection of the *Exo1* vectors and TALEN-NC showed significantly higher activity (25.9%) compared with TALEN-NC alone in the Surveyor assay (Figure 1D, E). Sequence analyses of the *Tyr* loci revealed similar mutation rates to the results of the Surveyor assay: 5.7%, 7.3%, and 17.7% in TALEN, TALEN-NC, and TALEN-NC + *Exo1* transfected cells, respectively (Table 1). There was no difference in the types of indel mutation or their sizes, which ranged from a 1-bp insertion to a 53-bp deletion centered over the TALEN recognition sites (Figure 1F–H).

***Exo1* increases the frequency of TALEN-induced gene disruption in rat zygotes.** To evaluate the gene targeting efficiency of TALENs in zygotes, we microinjected mRNA of the assembled Tyr-TALEN-NC with and without *in vitro* transcribed *Exo1* mRNA into fertilized rat eggs (Figure 2A, B). After 24 h, 30–40% of the TALENs-injected embryos differentiated normally into two-cell embryos with or without *Exo1*. PCR and sequence analyses on the two-cell embryos detected a mutation rate of 5.6% (1/18) in TALEN-NC and 28.6% (4/14) in TALEN-NC with *Exo1*, indicating that *Exo1* increases the frequency of TALEN-induced mutations in zygotes (Figure 2A). Interestingly, PCR and sequence analyses revealed that TALEN-injection into fertilized eggs could introduce homozygous mutations, which could not be detected by the Surveyor assay (Figure 2C, D). This means TALEN-induced mutations created by NHEJ could be induced at the one-cell stage, presumably during the S-phase (the DNA synthesis phase) of the cell cycle, in fertilized eggs.

Coinjection of TALENs mRNA with *Exo1* mRNA into embryos provides efficient generation of knockout rats. To generate knockout rats for the albino locus by TALENs, we again microinjected mRNA for TALENs or TALENs-NC into fertilized eggs of agouti DA rats. Of 328 TALEN-injected eggs, 126 two-cell embryos (38.4%) were transferred into the oviducts of pseudopregnant Wistar female rats, and 29 (23.0%) of these embryos were successfully carried to term (Figure 3A). However, no mutant pup was detected by sequence analyses of the targeted *Tyr* locus. Microinjection of TALENs commercially obtained from Cellectis (Paris, France) delivered two mutant pups among 30 born (6.7%) (Figure 3A). When we coinjected *Exo1* mRNA with TALENs-NC, 29 two-cell embryos were obtained from 68 injected eggs (42.6%) without obvious toxicity, and of 12 pups delivered (41.4%), three founders possessed mutations comprising 5- to 29-bp deletions (25.0%) (Figure 3B, C).

One male founder showed the albino coat-color phenotype over its entire body (Figure 3B), and sequence analyses revealed that this founder carried a homozygous mutation (a 29-bp deletion) at the *Tyr* locus (Figure 3C). When we crossed the founders with the DA strains, the TALEN-induced mutations were faithfully transmitted to the next generation. For example, a male G0 founder showing a mosaic coat-color phenotype was crossed with a DA female to obtain G1 heterozygotes. Subsequent intercrossing between G1 heterozygous males and females produced homozygous albino G2 offspring (Supplementary Fig. S1).

Discussion

As far as we know, this is the first report to show that coinjection of exonuclease *Exo1* with engineered nucleases, such as TALENs, could enhance the frequency of targeted gene disruption in zygotes, and could improve the targeting efficiency to generate knockout animals. This approach provides an easy, rapid and efficient method of generating knockout animals (Supplementary Fig. S2). For example, the custom design and assembly of TALENs and their validation by the SSA assay took 1–2 weeks. Direct injection of the engineered TALENs with pre-transcribed *Exo1* into embryos, transplantation into pseudopregnant foster mothers, and identification of TALEN-induced mutants took 1 month. A homozygous mutation producing an albino G0 founder was observed 3 weeks after birth. It will be interesting to determine how TALENs targeted both alleles to produce the homozygous mutation in zygotes, as has been observed in our previous experiments with ZFNs[13]. In addition, in our *in vitro* and *in embryo* experiments, no overt toxicity was observed when overexpressing *Exo1* in conjunction with TALENs. We also observed no effect of *Exo1* on the cell cycle and cell growth, or on embryo survival and embryo development. Although *Exo1* could increase the number of mutations at off-target sites, TALENs seem to have fewer off-target effects than ZFNs[21]. Although off-target effects might play a role in cell-based experiments, in animals such unknown mutations will be "washed out" by repetitive subsequent backcrossing with the parental strain.

It remains unclear how exonucleases enhance the efficiency of TALEN-induced gene disruption in zygotes. *Exo1* is a 5′–3′ exonuclease that has a major role in DSB-repair by 5′-strand resection of DSB-ends[22–26]. There are two major pathways for DSB-repair: NHEJ and HR. Recently, a third pathway, alternative NHEJ (altNHEJ), or microhomology mediated end-joining (MMEJ), was shown to repair DSBs in the absence or failure of the classical NHEJ (cNHEJ)

Table 1 | Surveyor assay and sequencing for TALEN-induced mutations in Rat-1 fibroblasts

			Sequence analysis		
Plasmid(s)	Cell No. (1×10^5)	Surveyor assay (%)	Mutations/Colonies	Mutation Rate (%)	Average del size (bp)
GFP	2.44 ± 0.58	0.44 ± 0.71	–	–	–
TALEN	2.81 ± 0.23	6.06 ± 0.56	5/96	5.2	14.2 ± 6.5
TALEN-NC	2.72 ± 0.33	11.04 ± 1.77	7/96	7.3	17.4 ± 6.8
TALEN-NC + Exo1	3.02 ± 0.35	25.86 ± 1.91	17/96	17.7	11.9 ± 2.6

A

Injected mRNA	Injected embryos	Two-cell embryos (%)	PCR-amplified (%)	Mutations (%)
TALEN-NC	70	21 (30.0)	18 (85.8)	1 (5.6)
TALEN–NC + Exo1	59	21 (35.6)	14 (66.7)	4 (28.6)

B

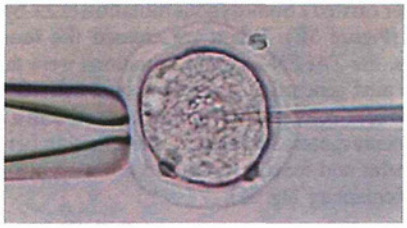

C

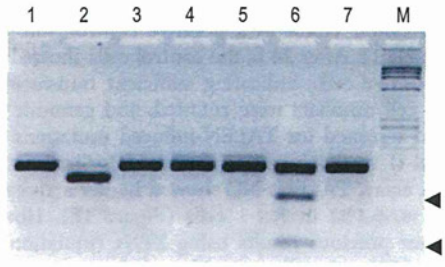

D

eT-NC-#8
TATAATAGCCATCAGGTTTT------TGGAAC---TGAGGGACCACTATTACGTAATCCT

eT-NC-Exo1-#2
TATAATAGCCATC---------(Δ24bp)---------AGGGACCACTATTACGTAATCCT

eT-NC-Exo1-#6
TATAATAGCCATCAGGTTTTATGTGATGGAACACCTGAGGGACCACTATTACGTAATCCT
TATAATAGCCATCAGGTTTTATGTG-----------CTGAGGGACCACTATTACGTAATCCT

eT-NC-Exo1-#10
TATAATAGCCATCAGGTTTTATGTGATGGAACACCTGAGGGACCACTATTACGTAATCCT
TATAATAGCCATCAGGTTTTATG------GAACACCTGAGGGACCACTATTACGTAATCCT

eT-NC-Exo1-#14
TATAATAGCCATCAGGTTTTATGTGATGGAACACCTGAGGGACCACTATTACGTAATCCT
TATAATAGCCATCAGGTT----------(Δ29bp)-----------ATTACGTAATCCT

Figure 2 | Targeted gene disruption by engineered TALENs in rat embryos. (A) Injection of TALEN-NC with or without *Exo1*mRNA into rat fertilized eggs. *Exo1* increased the efficiency of TALEN-induced mutations in zygotes by ~5×. (B) Microinjection of TALENs mRNA into male pronuclei of a fertilized egg. (C) Surveyor assay on the PCR products shows a TALEN-induced mutation as the digested products (arrowheads) in lane 6, but could not detect a homozygous mutation in lane 2. (D) Sequence analyses of the PCR products showed a 24-bp deletion in the homozygous alleles (eT-NC-*Exo1*-#2). Microhomologous sequences adjacent to the breakpoint are underlined.

pathway[27–29] (Figure 4). DSBs created by ZFNs or TALENs are generally repaired by cNHEJ with precise DNA-ends joining. When precise repair fails, or after the recession of DNA-ends by DNA exonucleases, DSBs would be repaired by altNHEJ, typically using closer microhomology sequences at both ends, thereby driving mutagenic end processing. Overexpression of *Exo1* probably increases DNA-end resections at the DSB-ends created by TALENs, thereby increasing the frequency of mutagenic DSB-repair via altNHEJ. To examine the effects of overexpression of *Exo1* on the NHEJ and HR pathways, we performed an NHEJ assay that measures the repair of I-SceI-generated DSBs via the NHEJ pathway[20,30] and an HR assay that measures the repair of I-SceI-generated DSBs via the HR pathway[20,31] (Supplementary Fig. S3). Those assays revealed that the *Exo1* significantly inhibited both the NHEJ pathway and the HR pathway in a wide variety of human cells (U2OS, HeLa, and MRC5), suggesting that the altNHEJ pathway would be enhanced in compensation, which might increase the frequency of the targeted gene disruption.

In conclusion, coinjection of exonucleases *Exo1* with TALENs provides an easy and efficient approach for gene knockouts in zygotes, and represents a promising breakthrough for gene targeting technologies applicable to various species.

Methods

Animals. All animal care and experiments conformed to the Guidelines for Animal Experiments of Kyoto University, and were approved by the Animal Research Committee of Kyoto University. Novel developed DA-*Tyr*^{em1Kyo} albino rats (NBRP-Rat No.0666) were deposited into the National Bio Resource Project – Rat in Japan (www.anim.med.kyoto-u.ac.jp/nbr).

Construction of TALEN plasmids and single-strand annealing (SSA) assay. The protocol for TALEN assembly was as previously reported[18,19]. Repeat assembly was conducted using a Golden Gate reaction, transformed into XL1-Blue competent cells and screened for precisely assembled clones by colony PCR using the pCR8_F1 and pCR8_R1 primers[19]. Constructed array plasmids and the appropriate last repeat were joined directly into the mammalian expression vectors, pcDNA-TAL or

A

Injected mRNA	Injected embryos	Two-cell embryos (%)	Pups (%)	♂	♀	Mutants (%)
TALEN	127	40 (31.5)	9 (23.0)	5	4	0 (0)
TALEN-NC	201	86 (42.8)	20 (23.3)	10	10	0 (0)
TALEN (Cellectis)	290	92 (31.7)	30 (32.6)	14	16	2 (6.7)
TALEN–NC + Exo1	68	29 (42.6)	12 (41.4)	7	5	3 (25.0)

B

C

gT-NC-Exo1-#1

TATAATAGCCATCAGGTT---------(Δ29bp)----------ATTACGTAATCCT

gT-NC-Exo1-#7

TATAATAGCCATCAGGTTTTATGTGATGGAACACCTGAGGGACCACTATTACGTAATCCT
TATAATAGCCATCAGG---------(Δ24bp)--------GACCACTATTACGTAATCCT

gT-NC-Exo1-#8

TATAATAGCCATCAGGTTTTATGTGATGGAACACCTGAGGGACCACTATTACGTAATCCT
TATAATAGCCATCAGGTTTTATGTGATG-----CCTGAGGGACCACTATTACGTAATCCT

Figure 3 | Efficient generation of knockout rats using TALENs with *Exo1*. (A) Microinjection of TALENs, TALENs-NC, TALENs from Cellectis, and TALENs-NC with *Exo1* into fertilized eggs of agouti DA rats. Coinjection of TALEN-NC mRNA with *Exo1* mRNA provided higher mutational efficiency (25%) in pups. (B) The white coat-color of an albino male rat (right) obtained by coinjection of TALEN-NC and *Exo1*. An agouti male (left) is a littermate. (C) Sequence analyses on founder rats showed a homozygous 29-bp deletion in *Tyr* (gT-NC-*Exo1*-#1). Microhomologous sequences adjacent to the breakpoint are underlined.

pcDNA-TAL-NC[18]. Final assembly, transformation and colony PCR screening for the second Golden Gate reaction were performed as previously reported[18,19].

The SSA assay was carried out as previously described[9]. The pGL4-SSA reporter vector was generated, containing inactive fragments of the luciferase gene, which bear 700-bp regions of homologous overlap and are driven by a cytomegalovirus (CMV) immediate-early enhancer/promoter. For the addition of TALEN target sequences, sense and antisense oligonucleotides, Sense: 5'- GTCGGATATAATAGCCATC-AGGTTTTATGTGATGGAACACCTGAGGGACCACTATTACGTAATCCTGG-AGGT-3', and Antisense: 5'- CGGTACCTCCAGGATTACGTAATAGTGGTCC-CTCAGGTGTTCCATCACATAAAACCTGATGGCTATTATATC-3', were annealed and inserted into *BsaI* sites between the dissected luciferase elements of pGL4-SSA. For the ZFN positive control, a ZFN expression vector, pSTL-ZFA36, was constructed, as previously described[9].

Rat *Exo1* cDNA cloning. To clone the rat *Exo1* cDNA, first strand cDNA was isolated using the oligo(dT)12-18 primer and SuperscriptII reverse transcriptase (Life Technologies, Carlsbad, CA, USA) synthesized from total RNA extracted from the brain of F344 rats by the Isogen reagent (Nippon Gene, Tokyo, Japan). RT-PCR was performed with the primers: 5'-GGGCCATGCCTGTTTATTC-3' and 5'-TGTTACCAGTGTGTTACCAGTCG-3'. RT-PCR products were inserted into pGEM-T Easy (Promega, Fitchburg, USA) and sequenced to confirm the sequence. For expression *in vitro*, the full-length cDNA was subcloned into pcDNA6.2/V5/GW/D-TOPO (Life Technologies).

Cell culture and transfection. Rat fibroblast-like (Rat-1) cells were obtained from the RIKEN BRC Cell Bank (Tsukuba, Japan, http://www.brc.riken.jp/lab/cell/english). The Rat-1 cells were cultured in DMEM (Invitrogen), supplemented with 10% FBS (fetal bovine serum, CBB) in a humidified atmosphere containing 5% CO_2 at 37°C. The cells (1×10^5) were suspended in 10 μl R buffer (supplied as part of the Neon Transfection System, Invitrogen), given 0.5 μg of each plasmid, and electroporated under the following conditions: pulse voltage, 1300 V; pulse width, 20 ms; and pulse

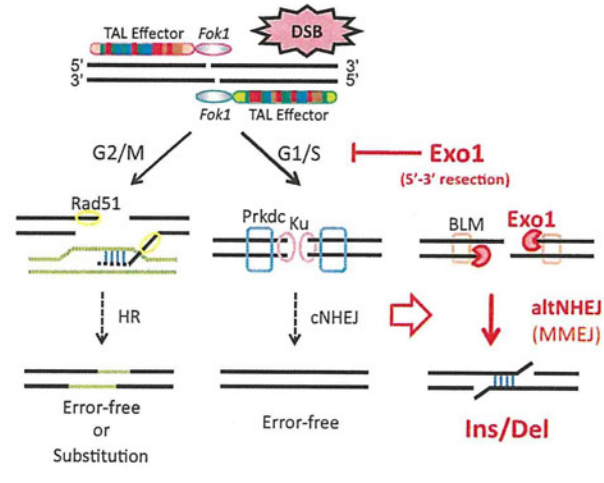

Figure 4 | Schematics of exonucleases (*Exo1*) functions in double-stranded break (DSB) repair pathways. Alternative NHEJ (altNHEJ), or microhomology mediated end-joining (MMEJ), generally repairs DSBs in the absence or failure of the classical NHEJ (cNHEJ) pathway[27–29]. Overexpression of *Exo1* induces increased recessions of DNA-ends at the DSB created by TALENs, which inhibits cNHEJ (See Supplementary Fig. S3) and enhances the mutagenic DSB-repair via altNHEJ, resulting in more indel mutations at the targeted gene.

number, 2 (program #15). Following electroporation, the cells were cultured in the medium described above without antibiotics for 24 h and then in the medium with antibiotics for 48 h. The *in vitro* transfer experiment was replicated three times.

Surveyor assay and DNA sequencing. For the Surveyor assay to detect TALEN-induced mutations, the SURVEYOR Mutation Detection Kit (Transgenomic, Omaha, NE, USA) was used in accordance with the manufacturer's protocol. Briefly, 72 h after electroporation, genomic DNA was extracted from the Rat-1 cells using Nucleospin (Macherey-Nagel, Düren, Germany). PCR was then performed using PrimeSTAR HS DNA polymerase (Takara Bio, Shiga, Japan), a high-fidelity enzyme, under the following conditions: 95°C for 1 min; followed by 95°C for 30 s, 68°C for 30 s, and 72°C for 1 min for 35 cycles. The PCR primers were as follows: 5′-TTGCATAAATTGGTTTTCACAGA-3′ and 5′-ATTTAAACATGAAAATAT-TACCTTCCA-3′. The PCR amplification products were heat denatured, digested by the Surveyor nuclease, and subjected to agarose gel electrophoresis to confirm TALEN-induced mutations.

For DNA sequencing analysis, the PCR products were subcloned into pCR4Blunt-TOPO plasmid vector (Life Technologies). Plasmids were extracted from the resultant *Escherichia coli* colonies for DNA sequencing. Sequencing was performed using the BigDye Terminator Cycle Sequencing Kit and an ABI PRISM 3130 Genetic Analyzer (Life Technologies).

Rat embryo culture. Pronuclear stage embryos were collected from DA/Slc females at 7 weeks of age that had undergone super-ovulation by injection with PMSG (Serotropin, Aska Pharmaceutical Co., Tokyo, Japan) and hCG (Gonatropin, Aska Pharmaceutical Co.). The GenomPlex Single Cell Whole Genome Amplification Kit (WGA4; Sigma Aldrich, St. Louis, MO, USA) was used to generate proprietary amplification of genomic DNA with universal oligonucleotide primers from a two-cell embryo. After purification, the single cell WGA products were analyzed the Surveyor assay and DNA sequencing analysis.

Microinjection of TALENs mRNA. To prepare mRNA of TALENs, TALEN-encoding expression plasmids were linearized with *Xho*I and extracted with phenol-chloroform by standard methods. To prepare the mRNA for *Exo1*, the *Exo1* plasmids were linearized with *Spe*I. Messenger RNA was transcribed *in vitro* using a MessageMax™ T7 mRNA transcription kit (Illumina, San Diego, CA, USA) and polyadenylated using a A-Plus™ Poly(A) polymerase tailing kit (Illumina). The resultant mRNA was purified using a MEGAClear™ kit (Illumina) and finally resuspended in RNase-free water at 10 ng/μl for each TALEN or *Exo1*. Approximately 2-3 pL of capped mRNA were injected into the male pronuclei of zygotes by microinjection[13]. The injected embryos were cultured in mKRB at 37°C with 5% CO_2 and 95% humidified air to promote their recovery. Surviving embryos were transferred to the oviducts of pseudopregnant Wistar females.

NHEJ and HR assays. NHEJ and HR assays were performed as previously reported[20,30,31]. *MRC5SV-pEJ* cells were used for the NHEJ assay. *U2OS-DRGFP*, HeLa-DRGFP and MRC5SV-DRGFP were used for the HR assay. To measure the repair of I-SceI-generated DSBs, 50 μg of the I-SceI expression vector (pCBASce) with or without a human *Exo1* expression plasmid (30 μg) was introduced into 5×10^6 cells by electroporation (GenePulser; Bio-Rad, Hercules, CA, USA). To determine the level of NHEJ or HR repair, the percentage of GFP-positive cells was quantified by flow cytometry (FACSCalibur; Becton Dickinson, Franklin Lakes, NJ, USA) 3 days after electroporation.

1. Carroll, D. Genome engineering with zinc-finger nucleases. *Genetics* **188**, 773–782 (2011).
2. Porteus, M. H. & Carroll, D. Gene targeting using zinc finger nucleases. *Nat Biotechnol* **23**, 967–973 (2005).
3. Rahman, S. H., Maeder, M. L., Joung, J. K. & Cathomen, T. Zinc-finger nucleases for somatic gene therapy: the next frontier. *Hum Gene Ther* **22**, 925–933 (2011).
4. Urnov, F. D., Rebar, E. J., Holmes, M. C., Zhang, H. S. & Gregory, P. D. Genome editing with engineered zinc finger nucleases. *Nat Rev Genet* **11**, 636–646 (2010).
5. Bogdanove, A. J. & Voytas, D. F. TAL effectors: customizable proteins for DNA targeting. *Science* **333**, 1843–1846 (2011).
6. DeFrancesco, L. Move over ZFNs. *Nat Biotechnol* **29**, 681–684 (2011).
7. Mussolino, C. & Cathomen, T. TALE nucleases: tailored genome engineering made easy. *Curr Opin Biotechnol* **23**, 644–650 (2012).
8. Scholze, H. & Boch, J. TAL effectors are remote controls for gene activation. *Curr Opin Microbiol* **14**, 47–53 (2011).
9. Ochiai, H. *et al.* Targeted mutagenesis in the sea urchin embryo using zinc-finger nucleases. *Genes Cells* **15**, 875–885 (2010).
10. Watanabe, T. *et al.* Non-transgenic genome modifications in a hemimetabolous insect using zinc-finger and TAL effector nucleases. *Nat Commun* **3**, 1017 (2012).
11. Ansai, S. *et al.* Targeted disruption of exogenous EGFP gene in medaka using zinc-finger nucleases. *Dev Growth Differ* **54**, 546–556 (2012).
12. Geurts, A. M. *et al.* Knockout rats via embryo microinjection of zinc-finger nucleases. *Science* **325**, 433 (2009).
13. Mashimo, T. *et al.* Generation of knockout rats with X-linked severe combined immunodeficiency (X-SCID) using zinc-finger nucleases. *PLoS One* **5**, e8870 (2010).
14. Cui, X. *et al.* Targeted integration in rat and mouse embryos with zinc-finger nucleases. *Nat Biotechnol* **29**, 64–67 (2011).
15. Miller, J. C. *et al.* A TALE nuclease architecture for efficient genome editing. *Nat Biotechnol* **29**, 143–148 (2011).
16. Certo, M. T. *et al.* Coupling endonucleases with DNA end-processing enzymes to drive gene disruption. *Nat Methods* **9**, 973–975 (2012).
17. Kuramoto, T. *et al.* Origins of albino and hooded rats: implications from molecular genetic analysis across modern laboratory rat strains. *PLoS One* **7**, e43059 (2012).
18. Sakuma, T. *et al.* Efficient TALEN construction and evaluation methods for human cell and animal applications. *Genes Cells* (in press).
19. Cermak, T. *et al.* Efficient design and assembly of custom TALEN and other TAL effector-based constructs for DNA targeting. *Nucleic Acids Res* **39**, e82 (2011).
20. Mashimo, T. *et al.* Generation and characterization of severe combined immunodeficiency rats. *Cell Rep* **2**, 685–694 (2012).
21. Mussolino, C. *et al.* A novel TALE nuclease scaffold enables high genome editing activity in combination with low toxicity. *Nucleic Acids Res* **39**, 9283–9293 (2011).
22. Bernstein, K. A. & Rothstein, R. At loose ends: resecting a double-strand break. *Cell* **137**, 807–810 (2009).
23. Huertas, P. DNA resection in eukaryotes: deciding how to fix the break. *Nat Struct Mol Biol* **17**, 11–16 (2010).
24. Longhese, M. P., Bonetti, D., Manfrini, N. & Clerici, M. Mechanisms and regulation of DNA end resection. *EMBO J* **29**, 2864–2874 (2010).
25. Mimitou, E. P. & Symington, L. S. DNA end resection--unraveling the tail. *DNA Repair (Amst)* **10**, 344–348 (2011).
26. Tran, P. T., Erdeniz, N., Symington, L. S. & Liskay, R. M. EXO1-A multi-tasking eukaryotic nuclease. *DNA Repair (Amst)* **3**, 1549–1559 (2004).
27. McVey, M. & Lee, S. E. MMEJ repair of double-strand breaks (director's cut): deleted sequences and alternative endings. *Trends Genet* **24**, 529–538 (2008).
28. Mladenov, E. & Iliakis, G. Induction and repair of DNA double strand breaks: the increasing spectrum of non-homologous end joining pathways. *Mutat Res* **711**, 61–72 (2011).
29. Symington, L. S. & Gautier, J. Double-strand break end resection and repair pathway choice. *Annu Rev Genet* **45**, 247–271 (2011).
30. Kobayashi, J., Kato, A., Ota, Y., Ohba, R. & Komatsu, K. Bisbenzamidine derivative, pentamidine represses DNA damage response through inhibition of histone H2A acetylation. *Mol Cancer* **9**, 34 (2010).
31. Pierce, A. J. & Jasin, M. Measuring recombination proficiency in mouse embryonic stem cells. *Methods Mol Biol* **291**, 373–384 (2005).

Author contributions

T.M. designed the work, produced all the data, and wrote the paper. T.K. and B.V. performed microinjection of TALENs into rat embryos. T. Sakuma and T.Y. constructed the TALENs. J.K. and Y.K. helped with *in vitro* experiments. T. Serikawa supervised the work. All authors read and corrected the manuscript before submission.

Additional information

Supplementary information accompanies this paper at http://www.nature.com/scientificreports

Competing financial interests: The authors declare no competing financial interests.

How to cite this article: Mashimo, T. *et al.* Efficient gene targeting by TAL effector nucleases coinjected with exonucleases in zygotes. *Sci. Rep.* **3**, 1253; DOI:10.1038/srep01253 (2013).

Zinc-finger nuclease-mediated targeted insertion of reporter genes for quantitative imaging of gene expression in sea urchin embryos

Hiroshi Ochiai[a], Naoaki Sakamoto[b], Kazumasa Fujita[b], Masatoshi Nishikawa[c], Ken-ichi Suzuki[d], Shinya Matsuura[a], Tatsuo Miyamoto[a], Tetsushi Sakuma[b], Tatsuo Shibata[c], and Takashi Yamamoto[b,1]

[a]Department of Genetics and Cell Biology, Research Institute for Radiation Biology and Medicine, Hiroshima University, Minami-ku, Hiroshima 734-8553, Japan; [b]Department of Mathematical and Life Sciences, Graduate School of Science, Hiroshima University, Higashi-Hiroshima 739-8526, Japan; [c]Laboratory for Physical Biology, RIKEN Center for Developmental Biology, Chuo-ku, Kobe, Hyogo 650-0047, Japan; and [d]Center for Marine Environmental Studies, Ehime University, Matsuyama 790-8577, Japan

Edited by Eric H. Davidson, California Institute of Technology, Pasadena, CA, and approved May 29, 2012 (received for review February 16, 2012)

To understand complex biological systems, such as the development of multicellular organisms, it is important to characterize the gene expression dynamics. However, there is currently no universal technique for targeted insertion of reporter genes and quantitative imaging in multicellular model systems. Recently, genome editing using zinc-finger nucleases (ZFNs) has been reported in several models. ZFNs consist of a zinc-finger DNA-binding array with the nuclease domain of the restriction enzyme FokI and facilitate targeted transgene insertion. In this study, we successfully inserted a *GFP* reporter cassette into the *HpEts1* gene locus of the sea urchin, *Hemicentrotus pulcherrimus*. We achieved this insertion by injecting eggs with a pair of ZFNs for *HpEts1* with a targeting donor construct that contained ~1-kb homology arms and a *2A*-histone *H2B–GFP* cassette. We increased the efficiency of the ZFN-mediated targeted transgene insertion by in situ linearization of the targeting donor construct and cointroduction of an mRNA for a dominant-negative form of *HpLig4*, which encodes the *H. pulcherrimus* homolog of *DNA ligase IV* required for error-prone nonhomologous end joining. We measured the fluorescence intensity of GFP at the single-cell level in living embryos during development and found that there was variation in HpEts1 expression among the primary mesenchyme cells. These findings demonstrate the feasibility of ZFN-mediated targeted transgene insertion to enable quantification of the expression levels of endogenous genes during development in living sea urchin embryos.

live imaging | quantitative biology

The phenotype and behavior of cells are largely determined by the expression levels of thousands of genes (1, 2). In some cases, the expression dynamics of specific genes also affect cell behavior (3). Therefore, to understand the molecular mechanisms of cellular events, it is necessary to quantify the expression of genes and their dynamics at the single-cell level. Techniques for insertion of a reporter gene into a genomic locus of interest and quantitative imaging of the reporter activities have been developed for this purpose (1, 4). By using these techniques in bacteria, yeast, and mammalian cells, it has been reported that a population of genetically identical cells can exhibit extensive cell-to-cell variability in the expression levels of many genes (3–6). However, for multicellular organisms, a universal technique for gene targeting and quantitative imaging has not yet been established in living animals.

Recently, a method for targeted gene editing using engineered zinc-finger nucleases (ZFNs) has been used in *Drosophila* (7), sea urchins (8), zebrafish (9, 10), plants (11), and human cultured cells (12, 13). ZFNs consist of a customized array of zinc-finger domains that bind to a specific DNA sequence and the nuclease domain of the restriction enzyme FokI. When two ZFNs bind to their associated target sequences in the appropriate direction, the nuclease domains dimerize, and a double-stranded break (DSB) is introduced. The ZFN-induced DSB can then be repaired with high efficiency by either homology-directed repair (HDR) or error-prone nonhomologous end joining (NHEJ) repair independently of a DNA template. Therefore, ZFNs can introduce a site-specific insertion or deletion at the DSB site after NHEJ repair (9, 11). Alternatively, ZFNs can produce defined genetic modifications, including the insertion of a reporter gene, near the site of the DSB by HDR using an exogenous targeting donor construct (7, 11). In animals, it has been noted that ZFN-induced DSBs are mainly repaired by NHEJ, and therefore ZFN-mediated targeted gene correction and transgene insertion are considered to be challenging (7, 14).

In the present study, we performed targeted insertion of a *GFP* reporter cassette into the endogenous *HpEts1* locus of the sea urchin, *Hemicentrotus pulcherrimus*, by injecting a pair of ZFNs with a targeting donor construct. The sea urchin embryo, which is transparent, simple, and readily accessible to experimental perturbations, offers a unique opportunity to study the regulation of morphogenesis during early development. In addition, in vivo quantitative imaging methodology at the cellular level has been established by using confocal laser scanning microscopy (CLSM) (15). Using CLSM, we measured the fluorescence intensity of GFP at single-cell resolution in reporter knock-in sea urchin embryos and found that there was variation in HpEts1 expression among primary mesenchyme cells (PMCs). These findings suggest that ZFN-mediated targeted transgene insertion can be used to quantify the expression levels of endogenous genes during development in sea urchin embryos.

Results

Targeted Transgene Insertion into the HpEts1 Locus Using ZFNs. To explore the possibility of inserting a reporter cassette into a genomic site of interest in the sea urchin, *H. pulcherrimus*, we selected the HpEts1L and HpEts1R ZFNs, whose target sites (5′-GGGGTTGACG-3′ and 5′-GATGATGACT-3′, respectively) are located upstream of the stop codon of the *HpEts1* gene responsible for PMC differentiation (16), by bacterial one-hybrid (B1H) and single-strand annealing (SSA) screenings (8) (Fig. 1*A* and Fig. S1). Zygotic expression of the HpEts1 transcription factor, which is encoded by the *HpEts1* gene, is detected in the nuclei of presumptive PMCs at the hatched blastula stage and in PMCs

Author contributions: H.O. and T.Y. designed research; H.O., N.S., K.F., K.S., S.M., T.M., and T. Sakuma performed research; H.O. and M.N. analyzed data; and H.O., T. Shibata, and T.Y. wrote the paper.

The authors declare no conflict of interest.

This article is a PNAS Direct Submission.

[1]To whom correspondence should be addressed. E-mail: tybig@hiroshima-u.ac.jp.

This article contains supporting information online at www.pnas.org/lookup/suppl/doi:10.1073/pnas.1202768109/-/DCSupplemental.

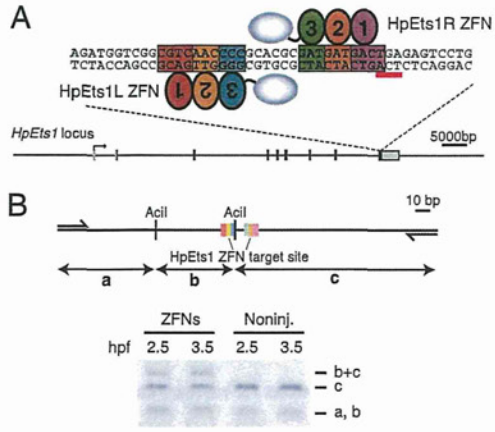

Fig. 1. The HpEts1 ZFNs introduce a DSB at a target site in sea urchin embryos. (*A*) The *HpEts1* gene showing the ZFN target site. A schematic representation of the *H. pulcherrimus* homolog of the *Ets1* gene (*HpEts1*) is shown. Exons are indicated by boxes. The gray and black boxes represent untranslated and coding regions, respectively. The bent arrow depicts the transcription start site. The ZFN-targeted sequence and the interaction site of the pair of ZFNs used in this study are shown. The red bar indicates the stop codon of the *HpEts1* gene. (*B*) Analysis of the mutations induced by ZFNs. A schematic representation of the *HpEts1* genomic region used for the PCR-based analysis is shown in *Upper*. The primer sites are indicated by arrows. The amplified region contains a target site for the HpEts1 ZFNs and two AciI sites. One of the AciI sites is within the HpEts1 ZFN target site. *Lower* shows a representative analysis of the PCR products. The PCR products amplified from genomic DNA extracted at 2.5 and 3.5 hpf from sea urchin embryos injected with the *HpEts1 ZFN* mRNAs (ZFNs) or noninjected control embryos (Noninj.) were purified, digested with AciI, and analyzed by agarose gel electrophoresis.

at the mesenchyme blastula stage (17, 18). To examine the activity of the HpEts1 ZFNs in sea urchin embryos, we amplified the DNA fragments around the target sites for the HpEts1 ZFNs by PCR using genomic DNA extracted from *HpEts1 ZFN* mRNA-injected embryos and control embryos at 2.5 and 3.5 h post-fertilization (hpf) and digested with the restriction enzyme AciI (Fig. 1*B*). An AciI-resistant fragment showing the introduction of mutagenesis was observed among the DNA fragments from the *HpEts1 ZFN* mRNA-injected embryos at 2.5 hpf (two- to four-cell stage), and the amount of this fragment was slightly increased at 3.5 hpf (four- to eight-cell stage), indicating that mutagenic NHEJ events occurred after the injection of the *HpEts1 ZFN* mRNAs. These findings suggest that the HpEts1 ZFNs introduced a DSB at their target site as early as 2.5 hpf.

Next, to examine the availability of ZFN-mediated targeted transgene insertion in sea urchin embryos, we prepared two targeting donor constructs, designated Ets-HRD (Fig. 2*A*) and Ets-HRD+T (Fig. 2*B*). The first targeting donor construct, Ets-HRD, contained ~1-kb homology arms and a *2A-H2B–GFP* cassette (2A is a self-cleaving peptide sequence) (19). Therefore, insertion of the reporter cassette into the *HpEts1* locus was expected to result in the expression of two polypeptides: full-length HpEts1 fused with the 17-amino acid sequence of the 2A peptide and H2B–GFP, which localizes to the nucleus where its fluorescence can be accurately quantified (20) (Fig. 2*A*). We confirmed that the 2A peptide mediated protein cleavage in sea urchin embryos by injecting mRNAs for 2A-linked constructs and performing Western blot analyses (Fig. S2). The other targeting donor vector, Ets-HRD+T, contained HpEts1 ZFN target sites at both ends of an Ets-HRD donor cassette and thus generated a linearized targeting donor in the embryos (Fig. 2*B*). In *Drosophila*, it was reported that the efficiency of ZFN-mediated targeted gene modification was increased by using

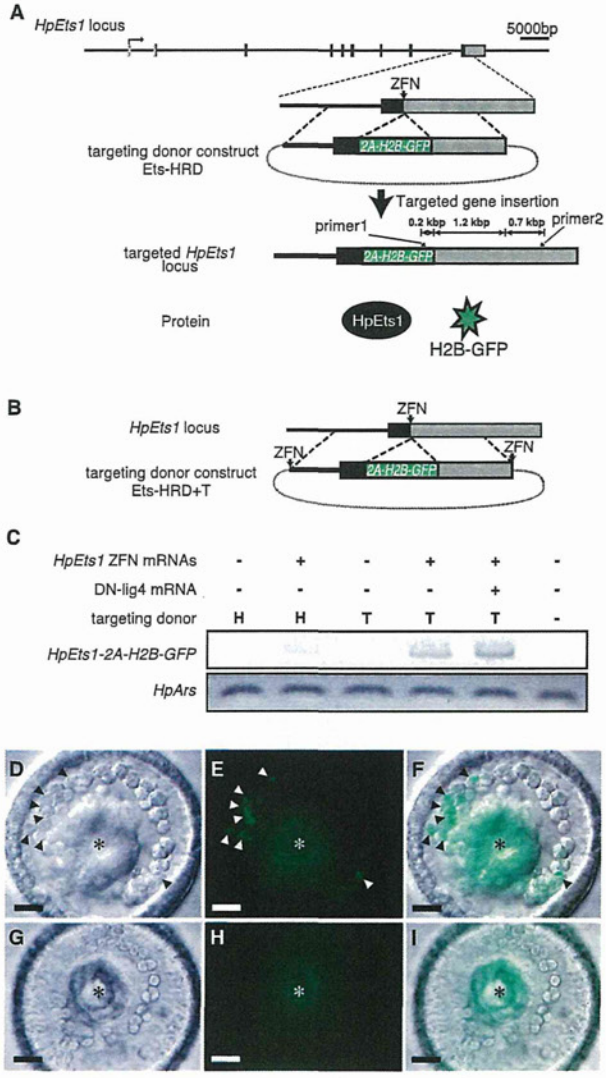

Fig. 2. ZFN-mediated targeted gene insertion. (*A*) Targeting donor construct (Ets-HRD) for insertion of the *2A-H2B–GFP* cassette into the *HpEts1* locus. The structure of the *HpEts1* locus and the targeted *HpEts1* allele are shown. The gray and black boxes represent coding and noncoding exons, respectively. Schematic representations of the proteins derived from the targeted *HpEts1* allele are also shown. These proteins are separated into the full-length HpEts1 protein and H2B–GFP during translation by the 2A self-cleaving peptide. The primer sites for the genomic PCR analysis are indicated. (*B*) Structure of the targeting donor construct Ets-HRD+T, which contains HpEts1 ZFN target sites at both ends of the Ets-HRD cassette. (*C*) Representative results of PCR-based genotyping analysis of the *HpEts1* locus. PCR was performed on genomic DNA extracted from embryos, which had been injected immediately after fertilization at 24 hpf. The primers used were either primers 1 and 2 (as shown in *A*) or primers to amplify the control gene *HpArs*. The PCR products were separated by gel electrophoresis. H and T represent injection of the Ets-HRD and Ets-HRD+T targeting donor constructs, respectively. (*D–F*) GFP-expressing embryo at 30 hpf injected with *HpEts1 ZFN* mRNAs, *DN-lig4* mRNA, and Ets-HRD+T. A representative embryo expressing GFP in the PMCs is viewed from the vegetal pole. (*G–I*) Noninjected control embryo at 30 hpf. (*D* and *G*) Bright field images. (*E* and *H*) Fluorescent images. (*F* and *I*) Merged images of *D* and *E* and of *G* and *H*, respectively. The arrowheads indicate GFP fluorescence in the nuclei of PMCs. Background autofluorescence is denoted by asterisks. (Scale bars, 20 μm.)

an extrachromosomal linear donor, which is linearized in situ, compared with a circular donor (21). In addition, we planned to repress NHEJ repair in the sea urchin embryos. For this purpose,

Table 1. Frequencies of GFP-expressing embryos

Targeting donor construct	*HpEts1 ZFN* mRNAs, each, pg	*DN-lig4* mRNA, pg	Mean GFP-expressing embryos, %*	Mean abnormal embryos, %*
Ets-HRD (40 fg)	—	—	0 (±0)	6.10 (±0.98)
Ets-HRD (40 fg)	1	—	1.86 (±0.60)	10.01 (±1.16)
Ets-HRD+T (40 fg)	—	—	0 (±0)	6.97 (±0.26)
Ets-HRD+T (40 fg)	1	—	12.01 (±0.77)	7.71 (±1.82)
Ets-HRD+T (40 fg)	1	5	15.92 (±1.55)	11.67 (±1.84)

There were three experiments for each targeting donor construct, and in each experiment, 200 embryos were injected.
*Values are mean percentages (averages of all trials) of GFP-expressing and abnormal embryos, respectively, with the SEM in parentheses.

we cloned a cDNA for the carboxyl-terminal tandem BRCT repeat of DNA ligase IV and prepared its mRNA (*DN-lig4*) with the expectation that overexpression of this mRNA would induce a dominant-negative effect, as reported in human cultured cells (22).

To validate the utility of ZFN-mediated targeted transgene insertion in the sea urchin, we injected several combinations of the targeting donor constructs, *HpEts1 ZFN* mRNAs, and *DN-lig4* mRNA, and we then performed PCR analyses using genomic DNA extracted from the embryos at 24 hpf (Fig. 2*C*). As expected, no PCR products were detected in the noninjected and donor-injected samples. In contrast, PCR products of the expected size were observed in the donor/ZFN-coinjected samples and were significantly increased in the Ets-HRD+T/ZFN-coinjected samples compared with the Ets-HRD/ZFN-coinjected samples. Furthermore, the amount of the PCR product was slightly increased in the embryos coinjected with *HpEts1 ZFN* mRNAs, Ets-HRD+T, and *DN-lig4* mRNA compared with those that did not receive *DN-lig4* mRNA. Sequencing of the PCR products confirmed the occurrence of the targeted insertion using the donor constructs (Fig. S3). Next, we examined H2B–GFP expression in the injected embryos using epifluorescence microscopy at 30 hpf (gastrula stage) and counted the numbers of H2B–GFP-expressing embryos (Fig. 2 *D–I* and Table 1). In some embryos, GFP fluorescence was observed in the nuclei of PMCs, in which HpEts1 is expressed (16, 17), and was never detected in other cell types. Consistent with the genomic PCR analysis, GFP-expressing embryos were more frequently observed after injection of Ets-HRD+T, *HpEts1 ZFN*s, and *DN-lig4* mRNAs than after injections with other combinations. These findings suggest that targeted transgene insertion using ZFNs is feasible in sea urchin embryos and that the combined use of donor constructs containing the target sites and DN-lig4 increases the insertion efficiencies.

Quantitative Imaging of Endogenous Gene Expression in Living Sea Urchin Embryos. In sea urchin embryos, in vivo quantification of *GFP* reporter gene expression at the single-cell level has been established by using CLSM (15). We predicted that application of this technique to embryos in which the *GFP* gene was knocked

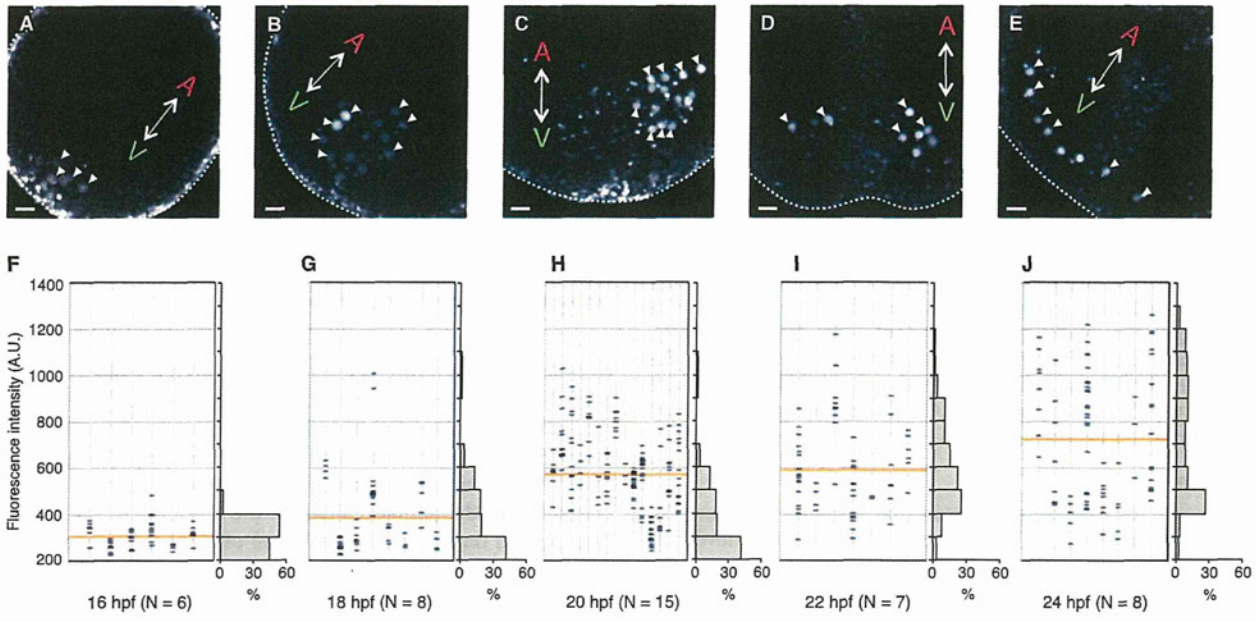

Fig. 3. Quantification of the mean fluorescence intensities in the nuclei of GFP-expressing cells during development. (*A–E*) Projections of *z*-stack images of GFP-expressing embryos. Representative GFP-expressing embryos injected with *HpEts1 ZFN* mRNAs, *DN-lig4* mRNA, and Ets-HRD+T were imaged at 16 (*A*), 18 (*B*), 20 (*C*), 22 (*D*), and 24 (*E*) hpf by using CLSM. The double-headed arrows indicate the animal pole (represented as a red A) and vegetal pole (represented as a green V). The white arrowheads indicate GFP fluorescence in the nuclei of PMCs. The white dotted lines indicate the outside cell surfaces of the embryos. (Scale bars, 10 μm.) (*F–J*) Distributions of the fluorescence intensity of GFP-expressing cells during development. The scatter plots on the left show the distributions of the GFP fluorescence intensities in individual embryos at 16 (*F*), 18 (*G*), 20 (*H*), 22 (*I*), and 24 (*J*) hpf. The orange lines represent the mean fluorescence intensities of GFP-expressing cells at each time point. The histograms on the right show the distributions of the fluorescence intensities of GFP-expressing cells at each time point.

into an endogenous genomic locus would enable real-time quantification of endogenous gene expression. To explore this hypothesis, we imaged embryos injected with Ets-HRD+T, *HpEts1 ZFNs*, and *DN-lig4* mRNAs at 16, 18, 20, 22, and 24 hpf using CLSM (Fig. 3 *A–E*). GFP fluorescence was observed in the nuclei of migrating PMCs at 16 and 18 hpf and in those of PMCs from 18 to 24 hpf. The numbers of GFP-expressing PMCs in the individual embryos ranged from 3 to 43 at 24 hpf (Table S1). Considering that an *H. pulcherrimus* embryo contains 55 ± 10 PMCs at this stage (23), the result suggests that ZFN-mediated targeted transgene insertion occurred at the developmental stage when there were 2–16 PMC-generating cells (Table S1).

As shown in Fig. 3, the mean fluorescence intensity in the cells increased during development. In addition, variation in the fluorescence intensity among cells increased after 18 h (Fig. 3 *F–J*). There are several possible reasons for this observation. First, it may have been caused by variation in the *GFP* copy number, because some GFP-expressing cells may only have had one *GFP* reporter gene monoallelically inserted into the *HpEts1* locus, whereas other GFP-expressing cells may have had two *GFP* reporter genes biallelically inserted into the *HpEts1* locus. To explore this possibility, we coinjected more than 200 fertilized eggs with *HpEts1 ZFNs* and *DN-lig4* mRNA together with Ets-HRD +T and Ets-HRD+mT containing an *mCherry* cDNA instead of the *GFP* cDNA (Fig. S4*A*). We obtained fluorescence images at 24 hpf by CLSM (Fig. S4*B*). In most fluorescent protein-expressing embryos, only one type of fluorescence was observed; 7% and 8% of injected embryos expressed GFP and mCherry, respectively. Although 2% of the embryos possessed both GFP- and mCherry-expressing PMCs, there were no embryos with GFP/mCherry double-positive PMCs. These findings suggest that the reporter construct is monoallelically inserted into the *HpEts1* locus in most fluorescent protein-expressing PMCs. Another possibility is that the variation in fluorescence intensity may have originated from differences in the endogenous HpEts1 expression levels between PMCs. To explore this possibility, we examined the fluorescence intensity of GFP-expressing PMCs and the ingression of PMCs in embryos injected with *HpEts1 ZFN* mRNAs, *DN-lig4* mRNA, Ets-HRD+T, and a moderate dose of an mRNA for a dominant-negative form of HpEts1 (ΔHpEts) (ref. 16; Fig. 4). We expected that the threshold level at which HpEts1 activates PMC differentiation would be raised by the expression of ΔHpEts, which lacks the activation domain and antagonizes native HpEts1 function by blocking its binding to the target site. If the GFP fluorescence intensity is related to the expression level of endogenous HpEts1, we expected that some presumptive PMCs expressing above-threshold levels of HpEts1 and H2B–GFP would differentiate into PMCs, whereas others with below-threshold levels of HpEts1 and H2B–GFP would not migrate into the blastocoel. Consistent with this hypothesis, significantly higher fluorescence intensity was observed in the nuclei of the PMC population than in the other GFP-positive cell population in the blastoderm (Fig. 4). These findings suggest that there is variation in zygotic HpEts1 expression among PMCs.

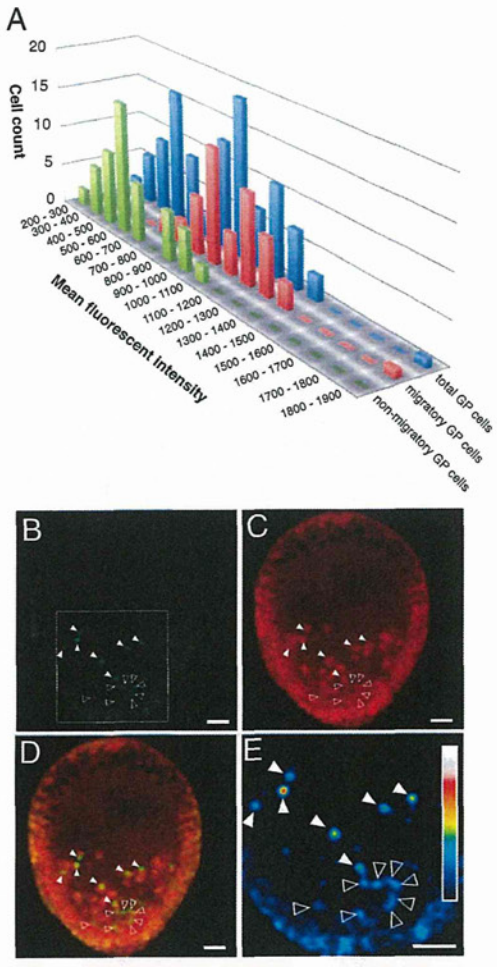

Fig. 4. Variation in fluorescence intensity among GFP-expressing cells. *HpEts1 ZFNs*, *DN-lig4* mRNA, Ets-HRD+T, and *ΔHpEts* mRNA were injected into fertilized eggs, and the fluorescence intensities of GFP-positive cells were quantified at 24 hpf. (*A*) Distribution of the GFP fluorescence intensities in migratory, nonmigratory, or total GFP-positive (GP) cells in embryos injected with a low dose of *ΔHpEts* mRNA. (*B–E*) Representative projections of *z*-stack images of a GFP-expressing embryo coinjected with *ΔHpEts* mRNA. *B*, *C*, and *D* show GFP, Texas Red, and merged images, respectively. (*E*) Pseudocolored and enlarged image of the area marked by the white square in *B*. *Inset* represents the pixel intensity profile. The filled and open arrowheads indicate GFP-positive cells ingressed and not ingressed into the blastocoel, respectively. (Scale bars, 20 μm.)

Discussion

In this study, we have demonstrated that targeted transgene insertion into the *HpEts1* locus can be efficiently achieved by cointroduction of ZFNs and a targeting donor construct in sea urchin embryos. Moreover, by combining this technique with fluorescence quantification, we were able to measure the expression levels of endogenous genes in living sea urchin embryos.

Targeted Transgene Insertion in Sea Urchin Embryos Using ZFNs. Insertion of the reporter gene into the target site was detected in embryos coinjected with the targeting donor construct and *ZFN* mRNAs, but not in embryos injected with the targeting donor alone. These findings indicate that spontaneous homologous recombination is a rare event in the sea urchin embryo and that a ZFN-induced DSB at the target site stimulates HDR, resulting in the induction of targeted transgene insertion at a detectable level. This result is in agreement with earlier work using *Drosophila* and mice (7, 14), suggesting that ZFN-mediated targeted insertion is feasible in model animals, although the efficiency of the insertion may depend on the species. Addition of ZFN target sites at both ends of the targeting donor cassette significantly increased the efficiency of ZFN-mediated targeted transgene insertion. In *Drosophila*, it was reported that an inserted donor was quite inefficient, an excised circular donor was better, and an extrachromosomal linear donor was best for HDR-mediated targeted gene modification (21). Therefore, it is considered that linearization of the targeting donor by ZFNs facilitates DNA strand invasion, which is required for HDR, or stimulates SSA, which involves extensive end processing to reveal complementary single strands in each repeat.

Cointroduction of *DN-lig4* mRNA increased the efficiency of ZFN-mediated targeted transgene insertion. It has been reported that DNA ligase IV, a major component of the NHEJ pathway, forms a complex with XRCC4 and seals DNA ends (22). Moreover, DSB repair can be biased toward HDR by disrupting the function of DNA ligase IV, resulting in an increase in the efficiency of targeted gene modification (7). Therefore, we hypothesized that in the sea urchin, inhibition of DNA ligase IV through the introduction of *DN-lig4* mRNA increases the propensity to repair ZFN-induced DSBs through HDR, resulting in enhanced efficiency of ZFN-mediated targeted transgene insertion. However, in the *Lig4* mutant of *Drosophila*, DSB repair was almost completely biased toward HDR, whereas in the sea urchin, the DN-lig4–mediated enhancement of the efficiency of ZFN-mediated targeted transgene insertion was modest (7). This result may arise because when DSBs are introduced by ZFNs, the DN-lig4 protein is not translated at a sufficiently high rate to completely inhibit the function of the endogenous DNA ligase IV. Therefore, the introduction of recombinant DN-lig4 and ZFN proteins into fertilized sea urchin eggs may enhance the efficiency of ZFN-mediated targeted transgene insertion.

Unintentional off-target cleavages are a potential problem with genome editing using ZFNs (24–26). Potential off-target sites are typically defined by scanning the genome for sites similar to the ZFN recognition sequences. However, because we could not directly search for putative off-target sites, owing to the lack of availability of the *H. pulcherrimus* genomic sequence, we searched for putative off-target sites that contained zero or one mismatches relative to each HpEts1 ZFN target site in the genome of *Strongylocentrotus purpuratus*, which is closely related to *H. pulcherrimus*. We found only one sequence containing one mismatch on *Sp-Ets1/2*, the ortholog of *HpEts1*. This finding implies that the HpEts1 ZFN target site on the *HpEts1* gene is a unique on-target site in the *H. pulcherrimus* genome and that insertion of the reporter gene into other genomic sites is a rare event when HpEts1 ZFNs are used in *H. pulcherrimus* embryos.

Quantitative Imaging of Endogenous Gene Expression in Living Sea Urchin Embryos. We successfully demonstrated visualization of endogenous gene expression in living sea urchin embryos by ZFN-mediated insertion of a *2A-H2B–GFP* cassette into the *HpEts1* locus. In this study, we used the 2A peptide, which is useful for balanced coexpression of multiple proteins from a single promoter, to avoid the synthesis of a fusion protein (19). Although a GFP fusion protein provides subcellular localization information as well as indicates the expression level of the gene of interest (1, 3), GFP may inhibit the function of its fusion partner. In our study, most of the reporter knock-in embryos exhibited normal development, and fluorescent signals were clearly detected in the nuclei of PMCs, suggesting that ZFN-mediated insertion of the *2A-H2B–GFP* cassette is a useful technique for quantitative imaging of gene expression at the single-cell level in developing embryos.

In the present study, we found variation in the expression levels of zygotic HpEts1 among PMCs. However, variation in the amounts of *HpEts1* mRNA and HpEts1 protein has not been detected by standard whole-mount in situ hybridization and immunostaining (16, 18). This variation may arise because these relatively low-sensitivity techniques cannot distinguish subtle variation in the expression levels. Another possibility is that substantial amounts of the *HpEts1* gene product, which was reported to be maternally expressed at abundant levels in whole sea urchin embryos (16), mask the variation in the amounts of the zygotic *HpEts1* gene product. In the latter case, it is difficult to distinguish between maternal and zygotic expression by conventional methods. In fact, although *HpEts1* mRNA is maternally expressed at abundant levels in the whole embryo during early development (16) and the mRNA and HpEts1 protein can be detected in presumptive PMCs and PMCs from the hatching blastula stage, it remains unclear whether this expression pattern is because of zygotic expression of HpEts1, selective degradation of maternal gene products except in presumptive PMCs and PMCs, or both. Therefore, ZFN-mediated reporter insertion is a useful technique for detecting the zygotic expression of an endogenous gene of interest. Our findings also show that PMC differentiation depends on the expression levels of zygotic HpEts1, suggesting that if maternal *HpEts1* mRNA and maternal HpEts1 protein remain in PMCs, they are functionally negligible. Further investigations are needed to understand the biological relevance of the variation in the zygotic HpEts1 expression levels among PMCs.

In most model animals, including the sea urchin, conventional transgenic methods, such as introduction of a reporter construct containing a *cis*-regulatory element of genes into embryos, are carried out to analyze the regulatory mechanism for the spatiotemporal expression of genes (27). However, in these methods, the reporter gene is randomly integrated into the genome, and its expression in embryos may be affected by positional effects, depending on the integration site (28). It was reported that the expression levels of some genes are regulated by distal regulatory elements (29). Therefore, it is uncertain whether sufficient regulatory elements required for endogenous expression are contained in the reporter constructs. In addition, the exogenous DNAs introduced into the sea urchin embryo are joined into concatemers, and multiple copies of them become incorporated into the chromosome (30), meaning that the reporter expression level is not always consistent with the endogenous expression level. In contrast, the combination of the ZFN-mediated targeted gene insertion and in vivo quantitative imaging techniques avoids the above-mentioned problems and enables quantification of the endogenous gene expression level in each cell in real time. The combination of ZFN-mediated targeted gene insertion and live imaging can potentially be applied to examine the relationship between the gene expression level in a cell and its fate. For example, it may be useful for elucidating the transfating mechanisms of presumptive blastocoelar cells to PMCs in embryos whose PMCs were depleted at the mesenchyme stage (31). The combined approach described here using sea urchin embryos might be extended to other multicellular model systems, such as nematodes and zebrafish, in which not only fluorescence imaging techniques but also ZFN-mediated genome modification techniques are available (9, 10, 32).

Materials and Methods

ZFNs targeting *HpEts1* were selected by B1H and SSA screenings as described (8); further information is included in *SI Materials and Methods*. Full descriptions of the constructions of the plasmids used in this study and the sea urchin culture conditions, as well as descriptions of the mRNA synthesis and microinjection, PCR-based genotyping assay, and imaging analysis, are detailed in *SI Materials and Methods* and Fig. S5. The sequences of oligonucleotides used in this study are listed in Tables S2 and S3.

ACKNOWLEDGMENTS. We thank Dr. Keith Joung for providing the pST1374 expression vector (Addgene plasmid 13426); Dr. Daniel Voytas for supplying the pc3XB-ZF60, pc3XB-ZF63, pc3XB-ZF64, and pc3XB-ZF70 vectors (Addgene plasmids 13196, 13199, 13200, and 13193, respectively); Dr. Scot Wolfe for providing the pH3U3-mcs reporter vector, pB1H2x2-zif268 plasmid, and USOΔhisBΔpyrFΔrpoZ bacterial strain (Addgene plasmids 12609, 184045, and 18049, respectively); Dr. Masato Kiyomoto for supplying live sea urchins; the Fisheries and Ocean Technology Center, Hiroshima Prefectural Technology Research Institute for supplying seawater; and the Cryogenic Center of Hiroshima University for supplying liquid nitrogen. This work was supported by Grant-in-Aid for Scientific Research on Innovative Areas 2020006 (to T.Y.) and Grant-in-Aid for Japan Society for the Promotion of Science Fellows 09J01990 (to H.O.). H.O. and T. Sakuma are Japan Society for the Promotion of Science Fellows.

1. Huh W-K, et al. (2003) Global analysis of protein localization in budding yeast. *Nature* 425:686–691.
2. Janes KA, et al. (2005) A systems model of signaling identifies a molecular basis set for cytokine-induced apoptosis. *Science* 310:1646–1653.
3. Cohen AA, et al. (2008) Dynamic proteomics of individual cancer cells in response to a drug. *Science* 322:1511–1516.
4. Sigal A, et al. (2006) Variability and memory of protein levels in human cells. *Nature* 444:643–646.
5. Elowitz MB, Levine AJ, Siggia ED, Swain PS (2002) Stochastic gene expression in a single cell. *Science* 297:1183–1186.
6. Raser JM, O'Shea EK (2004) Control of stochasticity in eukaryotic gene expression. *Science* 304:1811–1814.
7. Beumer KJ, et al. (2008) Efficient gene targeting in Drosophila by direct embryo injection with zinc-finger nucleases. *Proc Natl Acad Sci USA* 105:19821–19826.
8. Ochiai H, et al. (2010) Targeted mutagenesis in the sea urchin embryo using zinc-finger nucleases. *Genes Cells* 15:875–885.
9. Doyon Y, et al. (2008) Heritable targeted gene disruption in zebrafish using designed zinc-finger nucleases. *Nat Biotechnol* 26:702–708.
10. Meng X, Noyes MB, Zhu LJ, Lawson ND, Wolfe SA (2008) Targeted gene inactivation in zebrafish using engineered zinc-finger nucleases. *Nat Biotechnol* 26:695–701.
11. Shukla VK, et al. (2009) Precise genome modification in the crop species Zea mays using zinc-finger nucleases. *Nature* 459:437–441.
12. Urnov FD, et al. (2005) Highly efficient endogenous human gene correction using designed zinc-finger nucleases. *Nature* 435:646–651.
13. Hockemeyer D, et al. (2009) Efficient targeting of expressed and silent genes in human ESCs and iPSCs using zinc-finger nucleases. *Nat Biotechnol* 27:851–857.
14. Meyer M, de Angelis MH, Wurst W, Kühn R (2010) Gene targeting by homologous recombination in mouse zygotes mediated by zinc-finger nucleases. *Proc Natl Acad Sci USA* 107:15022–15026.
15. Damle S, Hanser B, Davidson EH, Fraser SE (2006) Confocal quantification of cis-regulatory reporter gene expression in living sea urchin. *Dev Biol* 299:543–550.
16. Kurokawa D, et al. (1999) HpEts, an ets-related transcription factor implicated in primary mesenchyme cell differentiation in the sea urchin embryo. *Mech Dev* 80: 41–52.
17. Fuchikami T, et al. (2002) T-brain homologue (HpTb) is involved in the archenteron induction signals of micromere descendant cells in the sea urchin embryo. *Development* 129:5205–5216.
18. Yajima M, et al. (2010) Implication of HpEts in gene regulatory networks responsible for specification of sea urchin skeletogenic primary mesenchyme cells. *Zoolog Sci* 27: 638–646.
19. Szymczak AL, et al. (2004) Correction of multi-gene deficiency in vivo using a single 'self-cleaving' 2A peptide-based retroviral vector. *Nat Biotechnol* 22:589–594.
20. Sprinzak D, et al. (2010) Cis-interactions between Notch and Delta generate mutually exclusive signalling states. *Nature* 465:86–90.
21. Beumer K, Bhattacharyya G, Bibikova M, Trautman JK, Carroll D (2006) Efficient gene targeting in Drosophila with zinc-finger nucleases. *Genetics* 172:2391–2403.
22. Wu P-Y, et al. (2009) Structural and functional interaction between the human DNA repair proteins DNA ligase IV and XRCC4. *Mol Cell Biol* 29:3163–3172.
23. Kominami T, Takaichi M (1998) Unequal divisions at the third cleavage increase the number of primary mesenchyme cells in sea urchin embryos. *Dev Growth Differ* 40: 545–553.
24. Gupta A, Meng X, Zhu LJ, Lawson ND, Wolfe SA (2011) Zinc finger protein-dependent and -independent contributions to the in vivo off-target activity of zinc finger nucleases. *Nucleic Acids Res* 39:381–392.
25. Gabriel R, et al. (2011) An unbiased genome-wide analysis of zinc-finger nuclease specificity. *Nat Biotechnol* 29:816–823.
26. Pattanayak V, Ramirez CL, Joung JK, Liu DR (2011) Revealing off-target cleavage specificities of zinc-finger nucleases by in vitro selection. *Nat Methods* 8:765–770.
27. Ochiai H, Sakamoto N, Momiyama A, Akasaka K, Yamamoto T (2008) Analysis of cis-regulatory elements controlling spatio-temporal expression of T-brain gene in sea urchin, Hemicentrotus pulcherrimus. *Mech Dev* 125:2–17.
28. Levis R, Hazelrigg T, Rubin GM (1985) Effects of genomic position on the expression of transduced copies of the white gene of Drosophila. *Science* 229:558–561.
29. Bulger M, Groudine M (2011) Functional and mechanistic diversity of distal transcription enhancers. *Cell* 144:327–339.
30. Hough-Evans BR, Britten RJ, Davidson EH (1988) Mosaic incorporation and regulated expression of an exogenous gene in the sea urchin embryo. *Dev Biol* 129: 198–208.
31. Sharma T, Ettensohn CA (2011) Regulative deployment of the skeletogenic gene regulatory network during sea urchin development. *Development* 138:2581–2590.
32. Morton J, Davis MW, Jorgensen EM, Carroll D (2006) Induction and repair of zinc-finger nuclease-targeted double-strand breaks in Caenorhabditis elegans somatic cells. *Proc Natl Acad Sci USA* 103:16370–16375.